CHALMERS

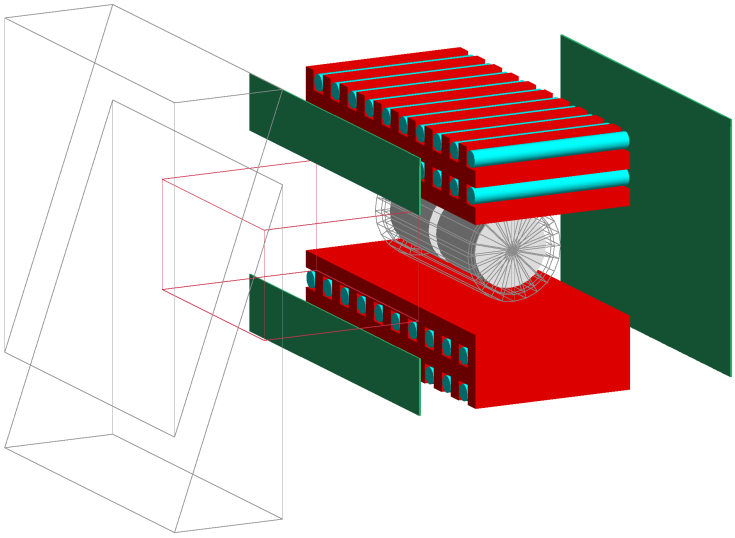

# Precalibrated Ion Beam Identification Detector

*Bachelor Thesis in Engineering Physics*

PHILIPPE KLINTEFELT COLLET
RIKARD LUNDMARK

Department of Fundamental Physics
*Subatomic Physics Group*
Chalmers University of Technology
Gothenburg, Sweden 2012

Chalmers University of Technology
Engineering Physics
Gothenburg

Department of Fundamental Physics
Subatomic Physics Group
Supervisor: Håkan Johansson

# Precalibrated Ion Beam Identification Detector

Bachelor Thesis

Philippe Klintefelt Collet
collet@student.chalmers.se

Rikard Lundmark
riklund@student.chalmers.se

**May 16, 2012**

**Abstract**

When conducting experiments with radioactive beams, a recurring problem is to identify the ions occurring in the beam. The identification process makes use of different detectors, which must be calibrated prior to usage — a process often requiring beam. This project investigates a concept and design for a help detector that can be calibrated without beam access. This pre-calibrated detector is to be used at the initial calibration of other detectors in the experimental setup, in order to save expensive beam time. The calibration in question is performed by, in turn, making absolute identifications of individual ions that have been detected by the main experimental setup. This identification is done by utilizing coincidence between $\beta$- and $\gamma$-decays in the detector and comparing measured $\gamma$-energies with tabulated values.

The detector was simulated using the `Geant4` toolkit, and the $\gamma$-energies were retrieved from the ENSDF database. It was found that using sufficiently low beam intensities, the detector could successfully identify most of the $^{17}$C ions in a beam composed of several different nuclides with mass and charge in the vicinity of those of $^{17}$C. The time of the identification was 13 hours, which is about one order of magnitude too long compared to what would be desirable in real-world experiments. Whether it is possible to further improve the design, and thereby increase the efficiency, will have to be concluded by further studies.

## Acknowledgements

This project would not have been possible without the help and support from many people.

First of all, we would like to thank our supervisor Håkan Johansson, for whose extensive support we are very grateful. Håkan showed an outstanding enthusiasm in the project and our work, and his comments, help and ideas were of great value throughout the length of the project. He was always available for interesting discussions and put much thought into the different parts of the project. A mail sent to Håkan would in general get an insightful reply within a few hours, regardless of the time of the day.

We are also grateful for the support and assistance from Carl Toft during the startup phase of the project during the summer 2011. Carl provided help in writing program code and was a valuable partner in discussions.

Furthermore we would like to thank Simon Lindberg for assistance with proof-reading the report. We would also like to mention the members of the Subatomic Physics Group at Chalmers University of Technology not directly involved in this project. Mentionable are the contributions of Andreas Heinz, who provided discussions concerning the `Geant4` toolkit, and Ronja Thies, who allowed us to use one of her images of the experimental setup at GSI.

The Authors, Göteborg, May 2012

# Contents

# 1 Introduction

In experiments using radioactive beams, it might be a problem to identify the ions passing the beam line. The detectors in use need to be calibrated to deliver absolute information and this in turn requires targeting the detectors with ions of a known kind (charge, mass) and velocity. Therefore it is of interest to use (help-)detectors that can be calibrated without a beam to simplify the absolute calibration and identification.

This bachelor thesis project revolves around the idea of a detector that could greatly facilitate and speed up calibrations of experiments that include radioactive particle beams. By use of the simulation toolkit `Geant4`, simulations of a proposed detector design are made and analysed. The flexibility of computer simulations has made it possible to alter detector configurations, and thereby to explore and optimize the design. In addition to this a number of additional programs have been written — for example a software for making search queries towards the ENSDF nuclide database.

## 1.1 Purpose and Scope

The purpose of this project is to study and evaluate a design concept for a self-calibrating ion beam identification detector. The overall aim of the project is to find answers to the following questions:

1. ***Will the proposed detector function?*** That is, is it possible to make ion identifications using the proposed working principle?
2. ***If it does function, how* well *does it function?*** That is, how can its functionality be quantified?

A detector of this type that is able to perform its task in a time of the order of 15 – 30 minutes may save important beam time as it operates in the presence of a particle beam while an experiment is being set up (refer to Figure 1).

It has also been of interest to investigate how the working concept can be optimized, — both in terms of cost and time of identification. It is reasonable to assume that for a higher cost it is possible to obtain a shorter time of identification, in which case a trade-off between the two has to be made.

The working principle that is evaluated puts certain requirements on the nuclides that are to be detected. A sub aim of the project is to identify the nuclides fulfilling these. For this purpose, a search program for the ENSDF nuclide database has been created. The search program, `ENSDF++`[1], is written in such a way that it easily can be reused or adapted for projects beyond this one.

## 1.2 Outline

In the following (Section 2) the physics and technical working principles of two relevant detector types, Germanium detectors and scintillators, are covered. Further, a background on the experiments conducted at GSI is given in Section 3, which also gives a

[1] The ENSDF++ search software is described in section 5.1.

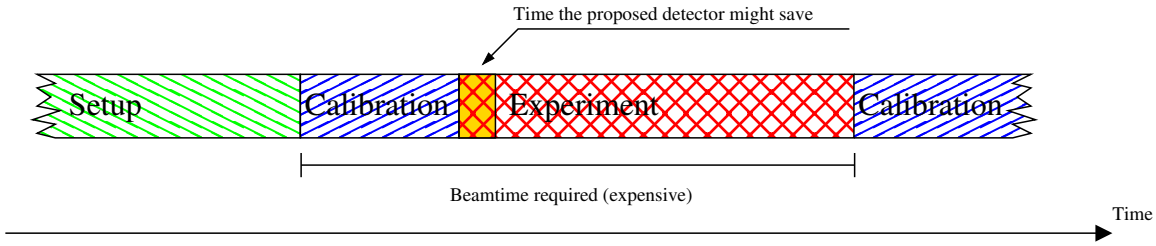


**Figure 1:** Sketch of the different phases in a typical experiment at GSI (not to scale). The proposed detector could, if it proves to work, save some beam time. This would mean more beam time availible for experimentation instead of calibration. Beam time is generally expensive, often coming at thousands of €/hour [4, p. 19]. Applying the methods widely used today, the time to identify the ion composition of a beam easily reaches 8 hours [20], corresponding to a considerable amount of money.

brief coverage of exsisting means of particle identification. The proposed detector design is first presented in Section 4. However, so is done without any evaluation of its functionality. Evaluation is covered in Section 5, where simulations (detector simulation, event mixer and analysis software) as well as the process of finding isotopes suitable for the working principle of the design are described. All presentation of results is concentrated to Section 6. In the last section the future of the detector is discussed and a conclusion is given.

# 2 Theoretical background on particle detection

A brief background on the two important detector types, scintillators and Germanium detectors, is given in this section.

## 2.1 Scintillator detectors

When a charged particle passes through matter, it loses energy. This energy loss is due to the excitation and ionization of atomic electrons in the material. A scintillator detector uses a scintillator, a material in which a small fraction of this excitation energy re-emerges as visible light during de-excitation [15, pp. 132-133]. This light is thereafter passed down into a photodetector that converts the light signal into a detectable electric impulse. This pulse is processed by the measurement electronics, which registers that a particle has deposited energy in the scintillator detector. Often the size of the pulse also gives information about the amount of energy lost.

If the velocity of the particle were known, this information could be used in conjunction with the energy loss to extract the charge of an ion passing the detector from Bethe's formula,

$$-\frac{dE}{dx} = \frac{4\pi}{m_e c^2} \cdot \frac{nz^2}{\beta^2} \cdot \left(\frac{e^2}{4\pi\varepsilon_0}\right)^2 \cdot \left[\ln\left(\frac{2m_e c^2\beta^2}{I\cdot(1-\beta^2)}\right) - \beta^2\right], \tag{1}$$

where $\beta = v/c$ and the quantities are as in Table 1 [10].

**Table 1:** Quantities in equation (1).

| **Quantity** | **Description** |
|---|---|
| $v$ | Velocity of the particle. |
| $E$ | Energy of the particle. |
| $x$ | Distance travelled by the particle. |
| $c$ | Speed of light. |
| $z$ | Particle charge. |
| $e$ | Charge of electron. |
| $m_e$ | Rest mass of the electron. |
| $n$ | Electron density in target. |
| $I$ | Mean excitation potential of target. |
| $\epsilon_0$ | Permittivity of vacuum. |

## 2.2 Germanium detectors

Germanium detectors consist of a single crystal of very pure Germanium with attached electrodes, over which a voltage is applied. The voltage creates a depletion area in the crystal, and when, for example, a secondary electron from a gamma interaction interacts with the electrons in the depletion area electron-hole pairs are created. Due to the applied voltage these reach the electrodes and cause a charge pulse that can be detected by the measurement electronics. The size of the charge pulse is proportional to the number of electron-hole pairs created in the material, which in turn is proportional to the deposited energy [12].

In order for the detector to work it needs to be cooled down to low temperatures. This may be done using either liquid nitrogen or cyogenic cooling. The latter is in general more expensive [24].

Germanium detectors have a depletion area that is much larger than, for instance, that of silicon detectors. This is the reason that these are used as gamma detectors in nuclear physics, since the gamma photons in question have relatively large penetration depths [13]. The interaction with the Germanium crystal can happen in three ways: photo absorption, Compton scattering and pair production [12]. These are described below, and an illustration is availible in Figure 3.

### 2.2.1 Photo absorption

Photo absorption means that the gamma photon deposits all its energy in an electron bound to an atom in the Germanium crystal. The kinetic energy of the electron then becomes the energy of the gamma photon minus the bound energy. Photo absorption is marked with green triangles in figure 3.

### 2.2.2 Compton scattering

Compton scattering means that the photon is spread against an electron which before the hit belongs to an atom, and thus transfers a part of its energy to this which is illustrated in figure 2. One can show that the correlation between the initial energy $E_\gamma$ of the photon, the kinetic energy $T_e$ of the electron and the scattering angle $\theta$ becomes [12, 14]:

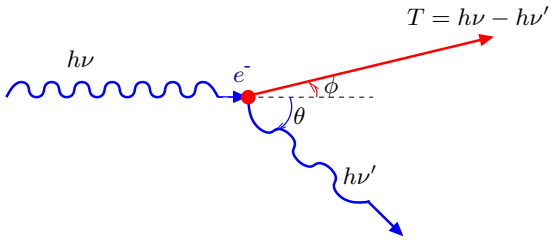


**Figure 2:** An incident photon is Compton scattered against an electron with the scattering angle $\theta$.

$$T_e = E_\gamma - E'_\gamma = \frac{E_\gamma^2(1-\cos(\theta))}{m_e c^2 + E_\gamma(1-\cos(\theta))}. \quad (2)$$

Compton scattering is marked using red circles in Figure 3.

### 2.2.3 Pair production

Pair production means that a photon is transformed into an electron-positron pair. This process requires that the gamma energies are higher than 1.022 MeV (corresponding to twice the rest mass of an electron) not to violate the principle of energy conservation. Pair production is marked using purple hexagons in Figure 3.

### 2.2.4 Combination

In reality one in general has a combination of the three processes above. This is illustrated with some common examples in figure 3. These are the following:

**Gamma photon 1** Compton scattered, and leaves the detector without depositing all its energy.

**Gamma photon 2** Compton scattered and photo absorbed. All energy is deposited in the detector.

**Gamma photon 3** Pair produced to an electron and a positron. The positron is annihilated with an electron, and the created photons are Compton scattered and photo absorbed. All energy is deposited in the detector.

**Gamma photon 4** behaves like gamma photon 3, but one of the photons from the annihilation leaves the detector before they have interacted. Deposited energy is incoming energy minus 511 keV.

**Gamma photon 5** behaves like gamma photon 3, but both the photons leave the detector before they have interacted. Deposited energy is incoming energy minus 1.022 MeV.

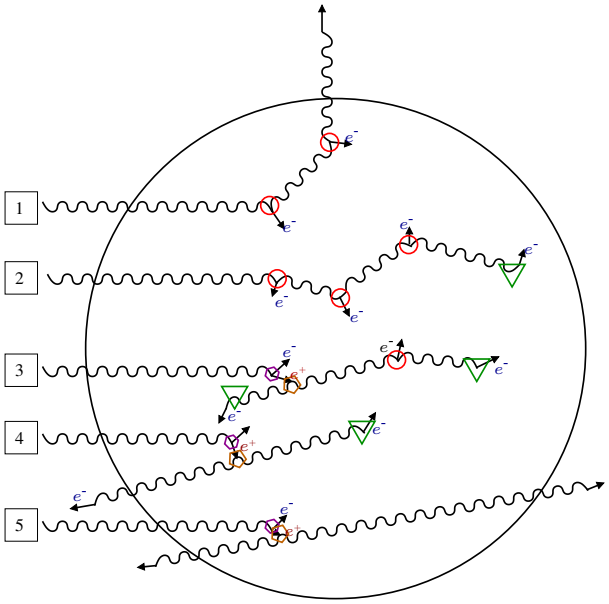


**Figure 3:** Illustration over some possible interactions between gamma rays and detector material for five incident gamma photons. Compton scattering is marked by red circles, photo absorption with green triangles, pair production with pink hexagons and annihilation with brown pentagons. The figures are more closely described in the text.

# 3 GSI Experiments

*GSI Helmholtz Centre for Heavy Ion Research GmbH (GSI)* is an accelerator based facility in Germany for heavy ion research, with which the Subatomic Physics Division at Chalmers University of Technology has a long standing cooperation [1, 19]. The intention is that the detector design evaluated in this thesis shall be able to be used at GSI.

A sketch of the experimental facility can be found in Figure 4. Ions are produced and sent either to experiments in the experimental hall, or to the SIS[2] synchrotron, where they are accelerated to relativistic energies. Thereafter they are sent directly or for exotic secondary ion production via the fragment separator (FRS) to a storage ring (ESR[3]) or a target hall. In Figure 4 target hall C is indicated [2, p. 6-8]. The detector under investigation is meant to be placed in the target hall behind the experimental setup not to disturb the experiment.

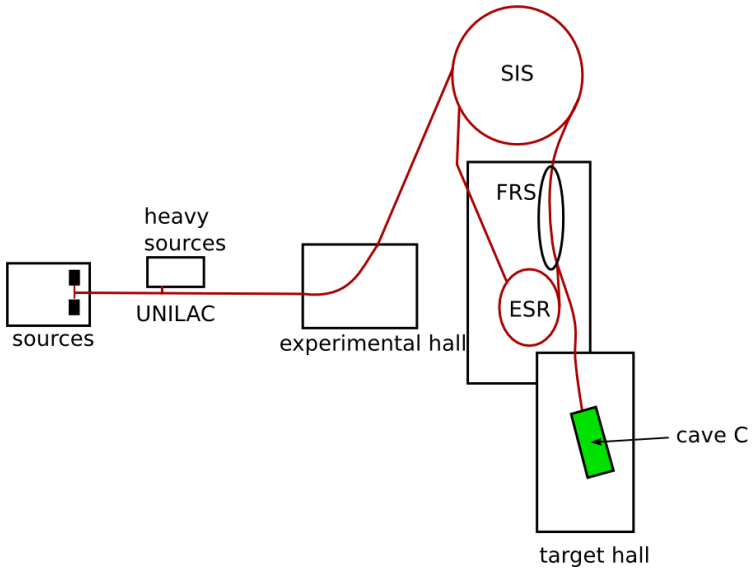


**Figure 4:** Sketch of a part of the experiment- and accelerator facility at GSI [2, p. 7]. Beam lines are marked in red. FRS (black ellipse) and Cave C (green rectangle) are marked. Chalmers subatomic researchers are doing the main part of their experiments in Cave C. The image is not to scale.

## 3.1 Determining Mass And Charge of Ions in an Experiment

During an experiment it is often necessary to identify the mass $A$ and charge $Z$ of a specific nuclide. This can be determined by using the known $B\rho$ value of the setup, the

[2]German: *SchwerIonen Synchrotron*, heavy ion synchrotron.
[3]Experimental Storage Ring.

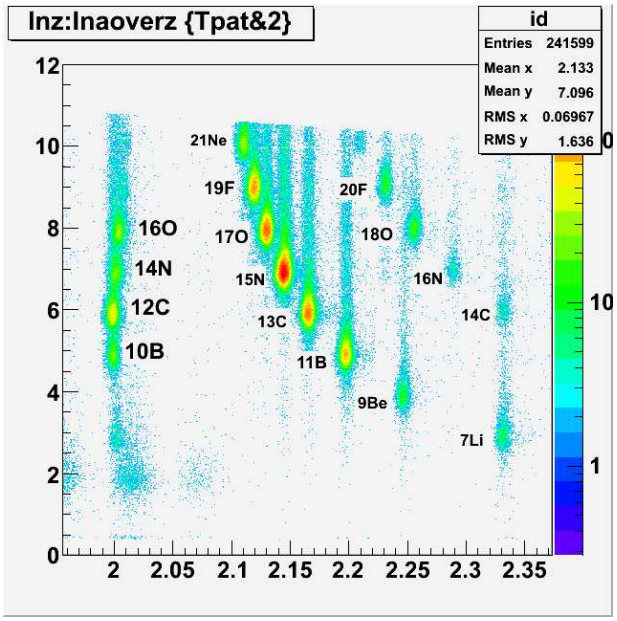


**Figure 5:** Example of scatterplot of $Z$ as function of $A/Z$ created live during an experiment [9].

velocity of the particles and the energy loss when passing known matter. A constant $B\rho$ value means a magnetic field with the same radius of curvature for particles passing through a constant magnetic field. The $B\rho$ value of the setup is determined by the FRS. This will only let ions with a specific $B\rho$ value through as only particles following a certain radius of curvature will come out at the end.

The velocity is determined by measuring the time of flight between scintillators placed far apart. This is done by registering the time it takes for a particle to pass from one scintillator to the other, which can be done with high resolution ($\sim 50\,\text{ps}$) [22]. Since the distance between the scintillators is known, the velocity of the nuclide can be obtained by dividing the distance by the measured time.

The energy loss is measured by determining the energy loss when the particles are travelling through a known material. This might for instance be a silicone diode [11]. When the energy loss and velocity is known, the charge can be extracted using Bethe's formula (1). Using the determined velocity and the $B\rho$ value, the $A/Z$ value can easily be determined. Thus we can obtain Figure 5, showing separation between the different ion species entering the experimental area.

In reality, the process of obtaining Figure 5 is not quite this easy. The value of $B\rho$ is not known exactly, the time-of-flight measurement might be uncalibrated and this also applies to the energy measurement. Thus some means of absolute calibration must be used [22].

## 3.2 Calibrating the Detectors

Once the $\frac{dE}{dx}$ and time-of-flight for the nuclides are known, these can be plotted in a graph. However, calibration is needed in order to obtain a graph as the one in Figure

5. A way to do this is to identify one of the clusters of data points as corresponding to a specific isotope. Then the points on the vertical and horizontal axes corresponding to the cluster can be directly assigned the values $Z$ and $A/Z$, respectively, of the identified isotope. How these cluster identifications can be done is described in Section 3.3.

### 3.2.1 Walk effect

A crux that sometimes has to be handled is the 'walk effect'. It is a severe problem that can lead to significant worsening of the time resolution of a detector signal. Without elimination of walk, for example the method of identification described in section 3.3.1cannot be applied, and therefore the calibration described above can in that case not be made.

The walk effect is the dependence of a time signal on its amplitude. The time $t'$ assigned by a discriminator from the signal of a certain active detector part can be viewed as

$$t' = t + f(e) \tag{3}$$

where $t$ is the real time of the event appearance, and $f(e)$ is a function containing the amplitude dependence of the measured time. Therefore, in order to perform a walk correction the function $f(e)$ must be determined and corrected for. If there are events with known $t$ available, the function $f(e)$ is easily determined [11]. For cases with unknown $t$, events with special properties can be used. This is a rather straightforward, but somewhat tedious process that will not be covered in this text[4].

## 3.3 Existing means of identification

Today there are several ways to identify particles in an obtained $\frac{dE}{dx}$ – time-of-flight graph. Two of the most important ones are the method of recognition of decay patterns, and use of the Isomer Tagging Detector available at GSI.

### 3.3.1 Recognition of decay patterns

One way to identify specific isomers in the $\frac{dE}{dx}$ – time-of-flight graph is to look for known decay patterns in the nuclide chart.

A typical example of this is the "$^8$Be hole". $^8$Be is not particle stable, and thereby has a very short half-life (81.9 as). Because of its short half-life, $^8$Be does not get out of the production target, much less reach the experimental setup, and a vacancy will occur in the $\frac{dE}{dx}$ – time-of-flight plot at the location where $^8$Be would otherwise come out, as is the case in Figure 5 at coordinate (2,4). If this vacancy can be identified, then neighbouring isotopes, such as $^{10}$B, can be identified as well, whereafter a calibration of the $\frac{dE}{dx}$ – time-of-flight graph can be made as described in Section 3.2.

[4] A full coverage of the algorithm used is given by Y. Aksyutina [11, pp. 26 – 29].

### 3.3.2 Isomer Tagging Detector

The Isomer TAGging detector (ITAG) provides another mean of making absolute identifications of certain nuclides, and thereby enabling calibration of the axes of the $\frac{dE}{dx}$ – time-of-flight plot. The ITAG, which is used today at GSI, utilizes a working principle that enables (and limits) it to detect isomers with a lifetime between 100 ns and 1 ms [3]. At GSI, isomer states are mainly produced for heavier nuclei at the isotope production before the FRS [18] (the placement of the FRS at GSI is illustrated in Figure 4). Though the ITAG may use their properties for identifying them, in many experiments isomers are an unwanted complication, as their excited states are likely to live through to later parts of an experimental setup before decaying. The main problem with isomers is that as they reach the experimental target, it is not certain whether they are in a metastable state or in the ground state. Not knowing this for sure makes analysis more difficult as two seemingly identical particles may show very different experimental properties.

The ITAG does in many aspects work in similar ways to those of the identification detector under investigation in this thesis (see Section 4 on the working principle of the proposed detector design). They share the principle of identification by high-precision measurement of $\gamma$-rays. The basic working principle of the ITAG can be summarized as [3]:

1. ***An isomer is implanted*** into a passive detector part situated near a Ge-detector.
2. ***The isomer $\gamma$-decays***, and the energy of the resulting $\gamma$-photon is measured with high precision by the Ge-detector.
3. ***The measured energy is compared*** with known $\gamma$-decay energy values tabulated in some reference table (such as the ENSDF database), and the isomer decaying is thereby identified.

A very important difference between the ITAG and the detector investigated in this thesis is what particles each detector can identify. While the ITAG identifies certain isomers, the proposed detector has the ability to identify nuclides which have the special property of $\beta$-decaying, with a certain half-life, into excited nuclear states.

Referring to Figure 9 it is seen that the isotopes that can be detected by the ITAG generally are not the same as the ones detectable with the proposed detector. In fact, the isotopes detectable by the PIBID only overlap those detectable by the ITAG in 22 out of 107 cases. Therefore, the two detectors should not be seen as rivals, but as complements to each other.

### 3.3.3 The Proposed Detector as a Means of Calibration

As a mean of calibration, the proposed detector provides information similar to that of the ITAG — namely absolute information coupling individual nuclides to experimental measurements.

# 4 The Proposed Detector Design

The idea and purpose of the detector design is to provide absolute information about the ion composition of particle beams, while also coupling the found ions with particle behaviour in an experimental setup. It is not expected to provide information about all particles by which it has been hit, with the proposed design it can only identify a few certain particles.

When a particle beam is directed towards it, as depicted in Figure 6, the detector produces a list of all detected ions bundled with time information associating each ion with certain events in the experimental setup from which they came. Therefore nuclear properties measured in the experiment can be assigned to each identified ion.

In practice there is uncertainty about the ion identifications (see Section 4.3 and Section 5.5), and therefore several such associations together with statistical means must be used to make the ion – experimental property association. If this is successful, however, the information can be used to make absolute calibrations of the main equipment of the experiment. To be able to make this sort of calibration of the main equipment is the sole cause of existence for the proposed detector design.

## 4.1 Design Overview and Working Principle

In Figure 6 the main parts A – F of the proposed detector design are shown:

**A and B** are scintillator plates whose purpose is to detect when particles pass through them.

**C** is a set of scintillator tubes in which incoming particles can be implanted. The scintillator tubes can detect at which time the implantations occur, as well as when particles inside them $\beta$-decay.

**D** is a Germanium crystal — the active part of a gamma detector with the ability to measure the energy of gamma photons with high precision.

**E** is a lead block whose purpose is to prevent incoming particles from hitting the Germanium detector, and thereby avoiding damage to the detector and interference in the measurements.

**F** represents two aluminum wedges used to control the energy at A, and thereby also the probability of implantation in the scintillator tubes C, of the particles that pass though them. By moving them together or apart the net aluminum thickness met by the incoming particles can be increased or decreased, respectively.

The identification of ions is made with the Germanium detector. If a gamma photon hits the Germanium crystal in coincidence with a beta decay in a scintillator tube, it can be concluded that the gamma photon was a direct result of the beta decay. If successfully measured by the detector, the energy of the gamma photon may be compared with tabulated values in the ENSDF nuclide database in order to be identified as a known

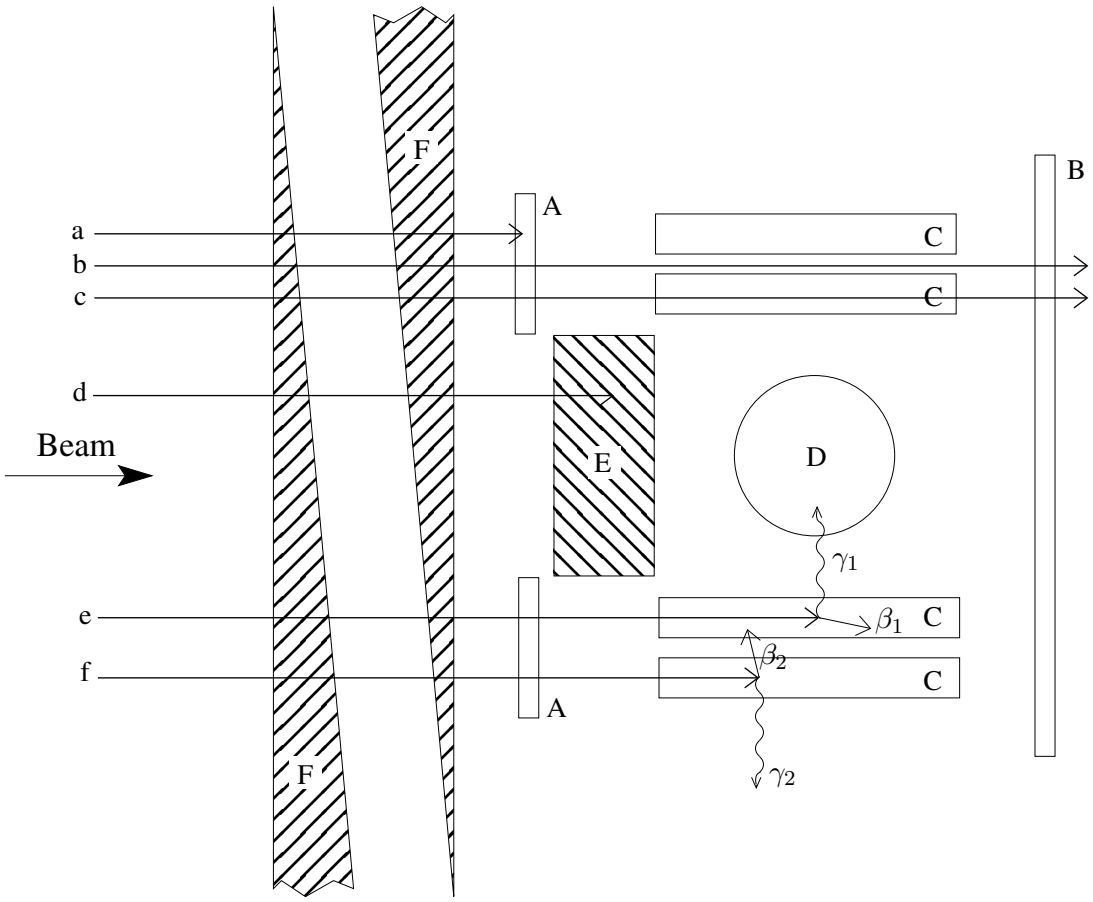


**Figure 6:** Sketch of the detector construction. A and B are plates made of scintillating material; C is a set of cylinders made of scintillating material parallel to the direction of the beam, placed side-by-side in the four groupings of C shown in the figure; D is a Germanium crystal as part of a Germanium detector; E is a rectangular box of lead; F represents wedges made of aluminum. $a - f$ are incident particles that interact with the detector; $\beta_1$ and $\beta_2$ are electrons resulting from the respective $\beta$-decays of $e$ and $f$; $\gamma_1$ and $\gamma_2$ are $\gamma$-photons resulting from the respective $\gamma$-decays of $e$ and $f$. $e$ may finally be identified.

$\gamma$-transition of some known nuclide. The coincidence between the beta- and gamma decays is critical, because without it there is no way of coupling the identification of a certain nuclide to the measurements of the experimental setup. The couplings between the experiment and individual scintillator tubes are made by time-stamping the events in the experimental setup as well as scintillator tube implantations. By then utilizing the known time of flight between the experiment and the scintillators, the principle of coincidence can be invoked. The whole experimental property – ion identification can be summarized as in Figure 7.

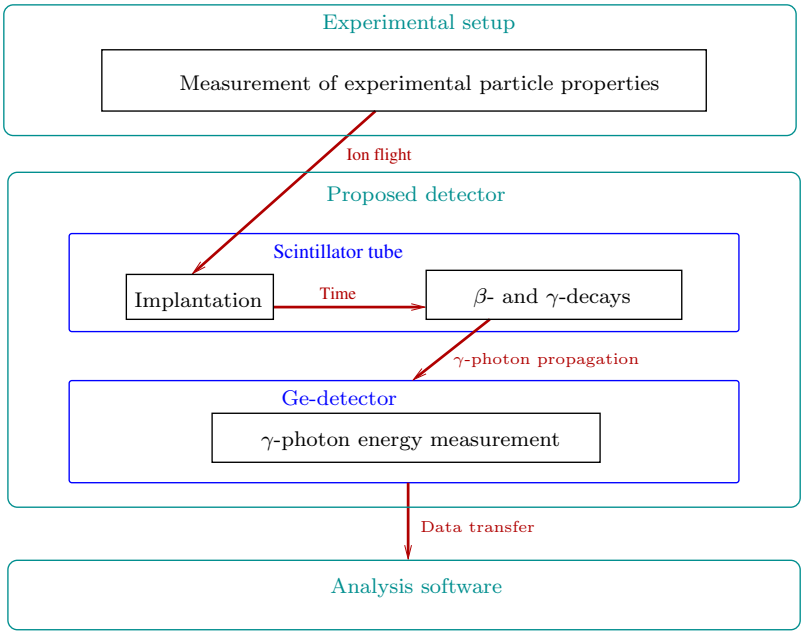


**Figure 7:** Working principle of the identification process. The flow depicted represents an ideal simplified case with no complications. In practice additional active detector parts are needed to handle the different problematic situations that may occur, as described in sections 4.2, 4.3 and 5.5. The colors in the figure are only for the purpose of grouping items to facilitate reading.

## 4.2 Examples of Particle – Detector Interaction

The sketch in Figure 6 of the detector construction illustrates several scenarios that include the particles $a$ – $f$

**Particle *a*** is stopped by scintillator plate A and never has a chance of being implanted into any of the scintillator tubes C. That is, $a$ is detected by the scintillator plate A but does not result in any energy deposition in C, and the event is therefore ignored.

**Particles *b* and *c*** both pass through both scintillator plates A and B, the conclusion that no implantation has occured is drawn, and the events are ignored.

**Particle *d*** is stopped by the lead block E and is nowhere detected.

**Particles *e* and *f*** are each implanted into respective scintillator tubes of C. A moment (in the order of 1–1000 ms) after their respective implantations they $\beta$-decay into nuclear excited states[5], shortly whereafter they each emit one or more $\gamma$-photons as they $\gamma$-decay from their respective excited states. It is, however, only the $\gamma$-photon $\gamma_1$ from particle $e$ that hits the $\gamma$-detector D, and whose energy thereby,

[5]This type of decay only occurs for certain nuclides; these are found in section 5.1

potentially, may be measured and compared with tabulated values in the ENSDF nuclide database for identification purposes (read further about this in section 5).

## 4.3 Some Complications and Solutions

The principle of correlating the $\beta$- and $\gamma$-decays using coincidence is powerful, but there are weaknesses to the method. Two important cases are described below.

### 4.3.1 Decay Particle – Detector Interference

When nuclides decay they will emit other particles. These may cause problems in the identification process as they may interact with the different parts of the detector.

Note, for example, that the electrons originating from $\beta$-decays potentially may interfere with the active parts of the detector. Apart from the detector part in which the $\beta$-decaying particle is implanted, the electrons may hit the Germanium detector D, scintillator plates A and B, as well as different scintillator tubes in C — just as the electron $\beta_2$ in Figure 6 does. This poses a problem from a particle identification point of view. The way the scintillators work (refer to Section 2.1) there is no accurate way to distinguish between a $\beta$-decay in a given scintillator tube and the detection of an electron crashing in from a $\beta$-decay in a neighboring detector component. This is an issue because it can potentially trick the analysis program. Picture the example of two ions being implanted into neighboring scintillator tubes before any of them $\beta$-decay, whereafter one of them $\beta$-decay in such a way that a resulting electron hits the other scintillator. With the time resolution of the scintillators the two events in the two scintillator tubes will be seen as instantaneous, so that at that point there will be no way of deducing which of the particles just decayed. Therefore, even if the gamma photon is detected, there will be no way of knowing which implanted particle it came from. There are however ways to cope with this type of problem. For example, a second $\beta$-decay in the tube with the non-decayed particle may not interfere with any other scintillators. Then the first $\beta$-decay can be identified as being that of the particle in the other scintillator tube. A practical measure that has been taken against this specific problem in the proposed design is the placement of shielding between the scintillators.

### 4.3.2 Multiple Implantations

Another important complication is the situation of two or more particles being implanted into the same scintillator tube before any of them have $\beta$-decayed[6]. In this case there is very little way of knowing which eventual $\beta$-decay belongs to which ion.

What can still be done is to look at the times between implantations. If a particular inter-implantation time is much longer than the half-lives of the involved particles[7] it can in most cases be concluded that the scintillator tube in question must actually have been

[6] This will later be referred to as a "double implantation" or "multiple implantation".

[7] These are often roughly known.

empty, and either the first particle was not really implanted or it $\beta$-decayed undetected[8] — that is, there was no multiple implantation after all. A true multiple implantation, however, is hard to deal with a constructive way. An option is to allow some erroneous identifications to occur, and associate all implanted nuclides in the scintillator with the following $\gamma$-decays.[9] This topic is further dealt with in Section 5.5.

## 4.4 Estimation of Construction Cost

The cost of constructing the detector can be subdivided into the cost of labor and the cost of materials. The labor cost will not be considered here, since it may be strongly dependent on the circumstances of construction.

The cost of materials is strongly dominated by the cost of the germanium detector(s) needed, since these are in general very expensive. The price range for a new detector ranges from approximately 10 k€ to more than 100 k€ [24]. The larger the crystal, the higher the price. The proposed detector would likely benefit from a larger crystal, which would thus drive the price towards the expensive end of the scale. One could also consider using two smaller crystals instead of one large, or just using one small at the cost of detector performance.

Except from the detector, one needs a cooling system to drive it. A cryogenic cooling system costs about 10 k€ [24]. This cost could be decreased to about 3 k€ if a cooling system using liquid nitrogen was to be used [24].

Considering these figures, it is reasonable to estimate the order of magnitude of the material cost of the detector construction to somewhere between 50 and 100 k€.

[8] Undetected $\beta$-decays are possible because $\beta$-particles have a continuous spectrum, and some will have energies that fall below the detector threshold.

[9] Note that the notion of knowing when all particles have decayed is a troublesome matter, as some must be expected to be missed by the detector. Handling this is a task for the data analysis software presented in Section 5.5.

# 5 Evaluation

The evaluation of the detector was conducted using computer-based methods, mainly programming. The first step was to identify and visualize the nuclides suitable for usage with the proposed detector. This was done by creating a search program for the ENSDF database and a plotting tool. When the nuclides were known, simulations could be done using Geant4. The results were analyzed accordingly. A sketch of the simulation-analysis is shown in Figure 8.

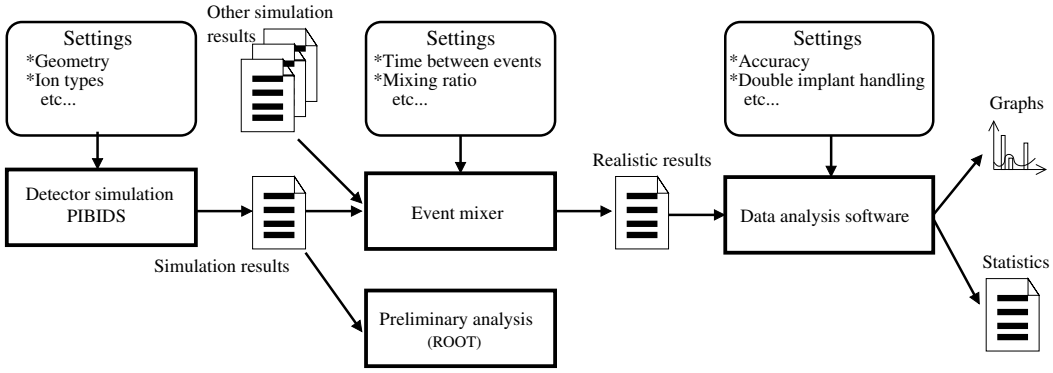


**Figure 8:** Sketch of the simulation-analysis process. For a specific detector geometry, simulations are run for different ion types. The results from the different simulations are mixed in the event mixer using a given set of settings, which for example determines the intensity of the ion beam and the mixing ratio between different ion types. The results from the event mixer are thereafter analyzed using a data analysis software. The output from the analysis software is graphs and statistics which are calculated using given settings.

## 5.1 Identification of Suitable Isotopes

A tool for searching the ENSDF database was developed using C++. The program was written with the intention of, with only minor modifications, being able to do searches in the ENSDF database other than the ones done in this project.

The program was named `ENSDF++`. Notable is that during the development of the software several syntax errors in the international nuclide database ENSDF were identified by the authors, and thereafter corrected [23]. For documentation and source code, see Appendix A.1. The software loads the ENSDF database into memory and processes it, whereafter one or more queries can be executed in order to obtain the desired information from the database.

For the purpose of this project the `ENSDF++`-software was specially adapted to find nuclides with beta decays that are followed by a gamma decay. The half-life of the beta decays was specified to between 1 ms and 1 s, and the probability of a specific gamma ray being emitted was specified to be at least 10 % when generating the nuclide chart in Figure 9 and the gamma list in Appendix B.

The ENSDF++-software had to compute the probabilities of gamma decay branches from other information found in the ENSDF database. The information in ENSDF only provides probabilities of specific gamma photons being emitted given a specific excited state. Furthermore there is no information about the level of excitation of the nucleus after decays, only before. Because of this the levels in the isotope dataset had to be searched for levels with energies approximately the gamma energy below the energy level that the nuclide had before the gamma photon was emitted. Thereafter an adjacency matrix was created, containing normed probabilities of transition from the $i^{th}$ to the $j^{th}$ level (corresponding to specific gamma rays). The beta branch strength was added as incoming intensities on each level, after which it was multiplied and summed from top to bottom in order to obtain the absolute probability of the emission of each gamma photon. The full details of this process are clear from the source code (Appendix A.1), more specifically from the class `DataQueryBetaGamma`.

A list of the found identifiable nuclides can be found in Appendix B. Notable here is that the probabilities of some gamma decays being emitted is above 100 %. The reason for this has been investigated and found to be that the probability of beta decays to different levels sometimes do not sum up to 100 %, which is likely due to the fact that ENSDF is a collection of experimental data and that there therefore might be experimental errors in the measurements.

The `ENSDF++` software also used the `mass.mas03`-file, a file containing experimental mass data of nuclides, in order to calculate Q-values of beta decays. Furthermore, a few additional single-purpose executables using the `mass.mas03`-part of the ENSDF software was created. These programs were used for creating lists of isotopes based on simple selection rules, which were then used in order to make the nuclide charts displayed in this report. The nuclide charts were painted using a Java program and a library for creating EPS images [16].

## 5.2 Detector Simulation

A detector simulation was created using the `Geant4` toolkit (see Figure 10). The simulation was named `PIBIDS` (Precalibrated Ion Beam Identification Detector Simulation).

The detector model is simulated for particles being fired towards it. For each fired particle, there might be a number of events. An event corresponds to measured energies in the different parts of the detector during a short time. The time used in the PIBIDS simulations were 1 $\mu$s. The time is long enough to include all interactions produced by either an incoming ion or beta decay[10]. It is also short enough to combine[11] extremely few implantations and decays. The events were collected and stored as measured energies in each of active parts of the detector together with information about which particle was fired and at what time the event was registered relative to the time that the particle was fired.

[10] Remember: speed of light is 30 cm/ns.

[11] Combining implantations or decays is unwanted, as then the information contained in the energy depositions are mixed up and obfuscated.

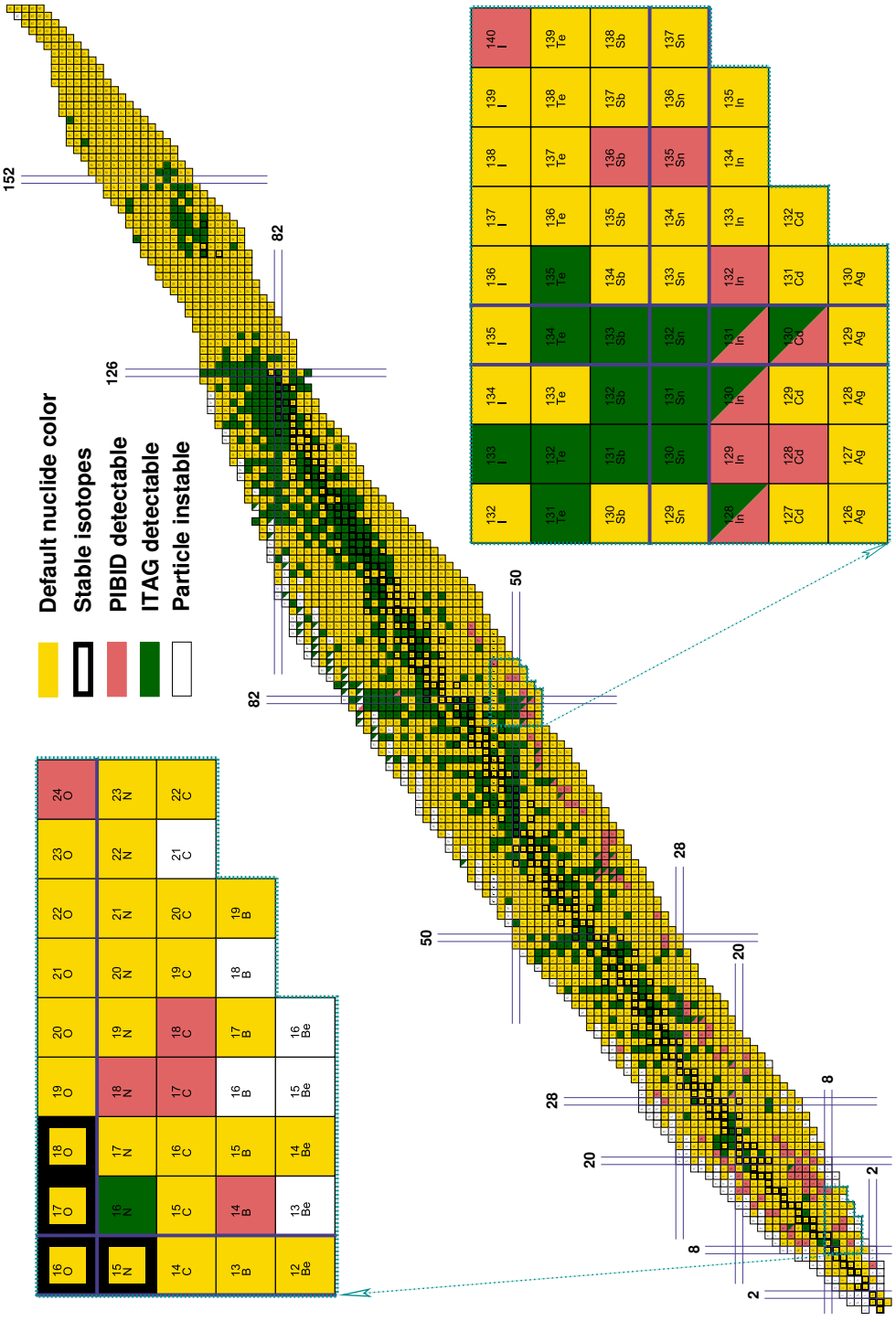


**Figure 9:** Nuclide chart exhibiting isotopes detectable by the PIBID and ITAG detectors. Color coding as explained in the figure. Note that the the nuclides detectable by the PIBID only overlap those detectable by the ITAG in 22 out of 107 cases.

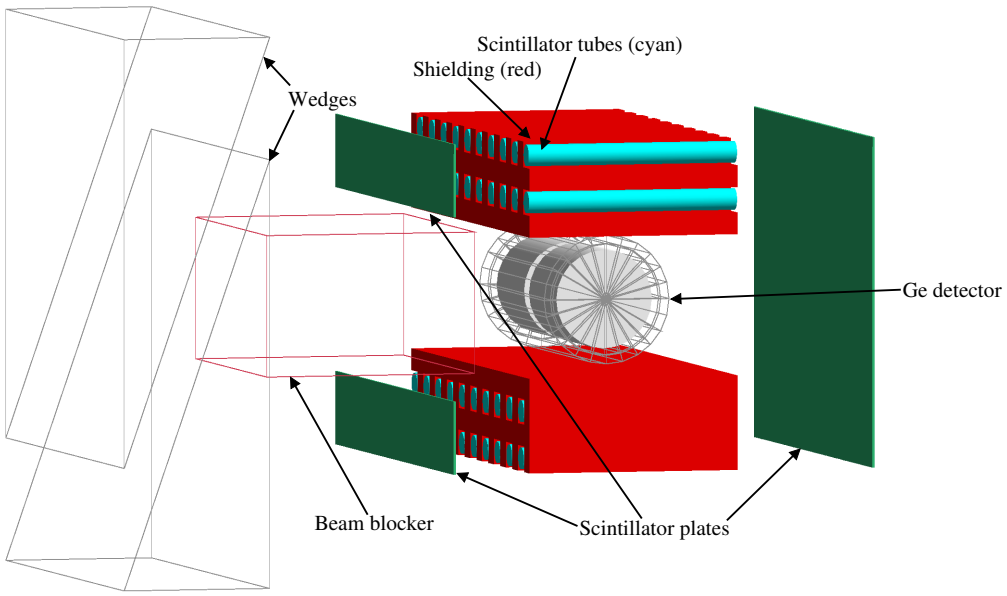


**Figure 10:** Illustration of the detector construction generated by Geant4. The grey transparent wedges are made of aluminium, the red transparent beamblocker is made of led, the red opaque shielding is by default made of quartz, the cyan scintillator tubes and the scintillator plates are made of plastic scintillator material. Compare to Figure 6.

The location of the documentation and source code of the PIBIDS is specified in Appendix A.2.

### 5.2.1 ATIMA

In order to set the effective thickness of the aluminium wedge degraders to a correct value, a software called `ATIMA` was utilized to estimate the required material thickness [8]. The calculated values were always spot-on the best degrader thickness (measured as the one generating most events) within an error of at most a few cm in material thickness. This was easy to verify by simply running simulations with wedge thickness values close to the values given by `ATIMA`.

## 5.3 Preliminary Analysis

A preliminary analysis of the data from `PIBIDS` could be done using `ROOT`, a data analysis framework. In order to do so the simulation results were converted to `ROOT`-format using a, for this purpose specifically written, software named `RootMaker`. The data could thereafter be viewed in histograms, and simple coincidence rules could be applied. This

was only a preliminary analysis, as the output directly from `PIBIDS` had limitations in similarity to real-world data. More about this in Section 5.4 below.

## 5.4 EventMixer Software

The output from `PIBIDS` consists of events grouped by individual fired particles, where each event in each group is stamped with a time relative to the impact time of the corresponding particle. All group of events, however, are generated and stored independently of each other. This would prevent one particle, including its byproducts, from affecting another. This is unrealistic and therefore and undesirable behaviour. To cope with this an event mixing software, named `EventMixer`, has been written in C++. It loads the simulation results from one or more PIBIDS result files and mixes the events according to the principle described in Figure 11. The output from the `EventMixer` is data that should mimic the output data from a real detector setup.

## 5.5 Data Analysis

The output from the event mixing software can be analyzed using a data analysis tool developed for that purpose. The data analysis tool was named `MDCAS` (Mixed Data Coincidence Analysis Software). It uses the "realistic" data from the event mixing software and compares the events with respect to time and affected active detector parts in order to obtain information about possible coincidences. The `MDCAS` has numerous settings concerning the behaviour of the analysis. For example, the handling of multiple implantations in scintillator tubes, the maximum wait time after an implantation and the acceptable gamma energies can be specified. Depending on the settings, different output is generated. Typically, detailed statistics about the implantations and decays are obtained together with `MATLAB` code for generating figures visualizing the measured coincident gamma energies in graphs. The data analysis tool was used for generating most of the results in Section 6. Figure 12 explains the association algorithm used to find a list list of implantation–decay coincidences from the mixed data. These coincidences contain information about the measured energies in different detectors, including the measured gamma energy. The contents of the coincidence list is split into several smaller lists depending on the type of the fired particle. It is assumed that the detectors in the experimental setup can determine which implantations comes from the same particle type by measuring time of flight and energy loss, as described in Section 3. Thereafter the gamma energies in each list are compared to known gamma energies in order to determine which nuclide is the most probable one. The energies are also plotted in a histogram in order to aid visual identification.

The data analysis software and documentation can be obtained using the instructions in Appendix A.5. During the association process, statistics about the data, such as the causes of different classifications, is collected. Example output from the data analysis software, including part of this statistics, is shown in Listing 1.

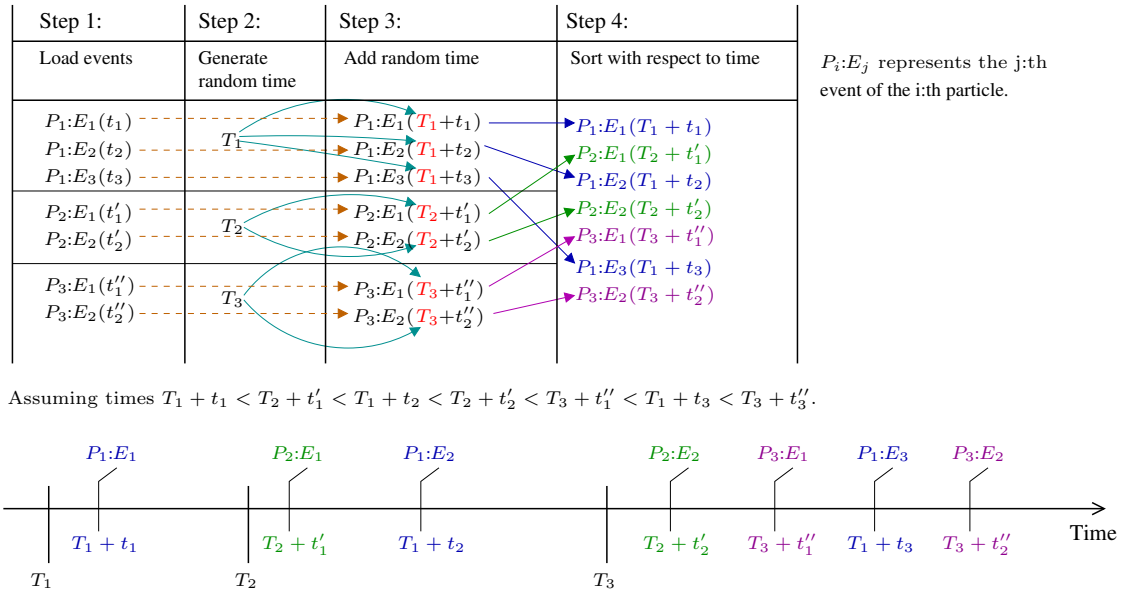


**Figure 11:** Working principle of the EventMixer software. The mixing can, a bit simplified, be subdivided into four steps:

*Step 1:* Events are loaded into memory from a simulation file created by PIBIDS. Each fired particle generally contributes with several events.

*Step 2:* For each fired particle a random time is generated in increasing order. The distribution of the difference between two subsequent random times is important, since this controls the frequency of the incident particles.

*Step 3:* To all event times the generated random time of their corresponding particle is added.

*Step 4:* The events are sorted in ascending order with respect to time.

The result will be events dispersed in time in a fashion similar to that on the timeline above. In reality the mixing is a bit more complicated; in order to limit memory usage data has to be read in and out of the software continously. The colors in the figure are only for the purpose of grouping items in order to facilitate reading.

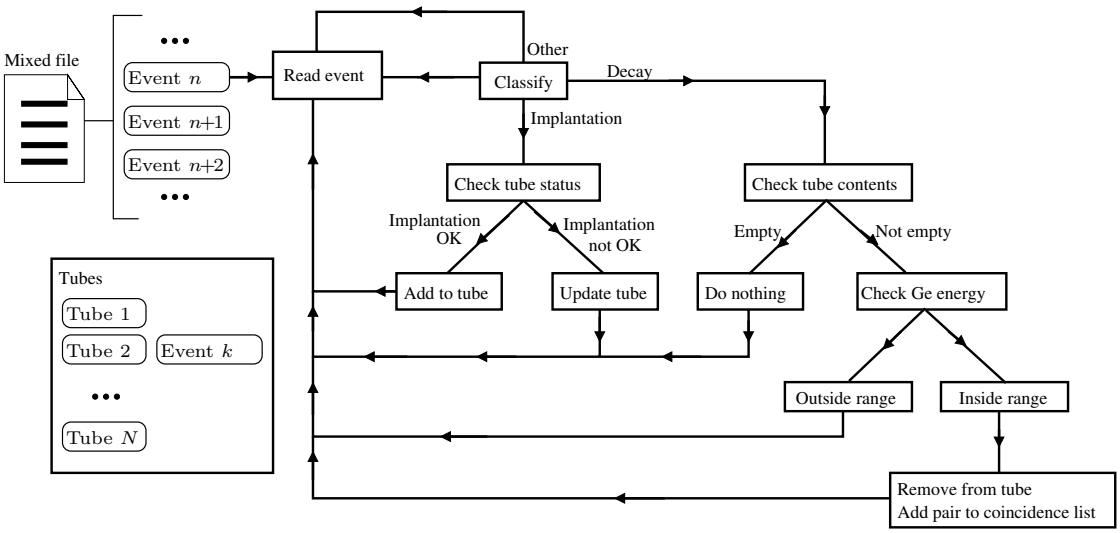


**Figure 12:** Simplified operating principle of the coincidence finding part of the data analysis software. A file from the event mixing software contains a large number of events (a typical order of magnitude might be $10^7$). The events cointains information of the measured energies in all detectors during that event, as well as the time of the event and information about which particle was fired to cause the event. These events are read one by one and processed by the analysis program. First an event is classified as either "implantation", "decay" or "other event". These are processed in the following way:

*Implantation:* The event is associated to the appropriate tube number in a list of all the scintillator tubes in the detector. If the tube was not ready for implantation (for instance, if it already held the maximum allowed number of implanted nuclides), then the incoming event as well as the events associated with the tube in question are discarded and the tube is marked as unavailible for implantations or decay for a certain amount of time.

*Decay:* If the tube from which the event came was empty or marked as unavailible the event is discarded. However, if the tube was availible and contained one or, if allowed by the settings, possibly more implanted nuclides, then the decay event is paired with the implantation events of all particles in the tube and added to a list of found coincidences. For the coincidences to be added, the measured gamma energy also has to be in the range of the acceptable $\gamma$-energies. Thereafter the implanted nuclides are removed from the tube, and it is marked as availible.

*Other:* The event is discarded, and if it did disturb any implanted particle that scintillator tube is marked as unavailible for implantation or decay for a certain amount of time.

After the entire mixed file has been processed, the list of found coincidences is further processed.

**Listing 1:** Example output from MDCAS.

```
++++++++++++++++Analysis settings:++++++++++++++++
Coincidence file:_____________________________AnalyzedResults/Report_C17area↩
    /Cd1e9D19e8.m
Time distribution file:_____________________AnalyzedResults/Report_C17area↩
    /Td1e9D19e8.m
Mix file (data to analyze):_____________________MixedResults/↩
    Report_C17area_finished/9e8.txt
Gamma data file:_____________________________Gammalista.txt

Tolerance (MeV):_____________________________0.003
Background tolerance (MeV):_____________________0.05
#Multi-implantations allowed:_____________________1
Number of scintillator tubes:_____________________40
Number of tubes per row:_____________________10
Ge detector epsilon (MeV):_____________________0.05
Beta detector epsilon (MeV):_____________________0.5
Domination ratio:_____________________________1000
Minimum Ge energy (MeV):_____________________0.5
Maximum Ge energy (MeV):_____________________3
Maximum decay wait (ns):_____________________1e+09
Decay cut (ns):_____________________________1e+20
Force correct identification:_____________________no
A range:_____________________________________5-25
Z range:_____________________________________2-15
Display detector count:_____________________yes
Display info about ID failures:_____________________no

=====================Statistics:=====================
# events processed:_____________________________6715955
Time of last implantation: _____________________25days 4hours 57minutes 24↩
    seconds
Classification of events:
--->#implantations:_____________________________470822
# Correct implantations:_____________________465900
# Double hits:_____________________________4922
--->#decays:_____________________________972305
# Non-associated decays:_____________________606531
# Decays without Ge-hit:_____________________75261
# Correctly connected implant-decay:_____________286260
# Incorrectly connected implant-decay:_____________79514
--->#other:_____________________________5272828
# Destroyed by other:_____________________19510

Reasons for other-classification:
Particle went through FSP and BSP:_____________604360
Particle through FSP but no implant:_____________2099514
Particle through FSP but implant in several tubes:1522
Particle not through SP, and no tube:_____________1320095
Particle not through SP, and several tubes:_____27699
Particle through BSP, not FSP, no tube:_____________1210764
Particle through BSP, not FSP, several tubes:_____25
Particle through BSP, not FSP, one tube:_____8849

Found coincidences:_____________________________8779
# correct:_____________________________________7247
Ratio:_____________________________________82.5493%
```

# 6 Results and discussion

Numerous simulations were run. In the simulations the isotope $^{17}$C was mainly used. In one case the surrounding nuclides were mixed together with $^{17}$C in order to make the identification process more realistic. There were multiple reasons for the choice of $^{17}$C:

- Neither $^{17}$C nor its neighbour nuclides are isomers. Thus the ITAG detector (see Section 3.3.2) would not be able to identify it.
- It is not particularly easy to identify, since the gamma photons emitted have relatively low probabilies. Thus it would yield realistic evaluation results.
- It is a light nucleus, and as such in a region of specific interest for the research conducted by the subatomic physics group at Chalmers University of Technology [21].

Particles hitting the detector have constant $B\rho$ value, which means they all have passed a constant magnetic field ($B$) with approximately the same radius of curvature ($\rho$) [17]. The values of $B\rho$ were calculated for a certain type of incident ions using a specific energy. This value was then used to calculate which incident energies the other particles in the mixture were to have.

The detector simulation had the standard settings shown in Table 2. Each simulation needed a different set of settings, and the standard settings were therefore overridden by simulation specific settings in each case. These overridden settings are described for each simulation.

The results of a series of simulations are accounted for in the following sections.

**Table 2:** Standard detector settings during the simulations. These settings are used for all simulations, unless other settings are specified. When other settings are specified they always override these settings.

| Parameter | Value | Description |
|---|---|---|
| Scintillator tube diameter | 10 mm | The diameter of the scintillator tubes. |
| Scintillator shielding gap | 0.5 mm | The gap between the scintillators and the shielding. |
| Number of scintillators per row | 10 | |
| Number of scintillator rows | 2 | Number of rows on each side of the detector. |
| Scintillator tube length | 10 cm | The length of the scintillator tubes (and of course also shielding). |
| Scintillator plate thickness | 1 mm | Thickness of scintillator plates. |
| Shielding thickness | 10 mm | Thickness of shielding between scintillator tubes. |

Continued on next page

**Table 2 – continued from previous page**

| Parameter | Value | Description |
|---|---|---|
| Top shielding thickness | 10 mm | Thickness of shielding between the scintillator rows. |
| Germanium crystal radius | 2.3 mm | |
| Germanium crystal length | 5 cm | |
| Germanium detector shell outer radius | 3 cm | |
| Germanium detector shell inner radius | 2.5 cm | |
| Number of Germanium crystals in detector | 2 | |
| Beam blocker thickness | 15 cm | |
| Shielding beam blocker thickness | 2 cm | |
| Wedge thickness | 50 cm | |
| Wedge length | 80 cm | |
| Effective degrader thickness | 36 cm | |
| Plate shield spacing | 5 mm | Spacing between shielding beam blocker and scintillator plates. |
| Scintillator material | Plastic | |
| Shielding material | Quartz | |
| Germanium detector shell material | Aluminium | |
| Beam blocker material | Lead | |
| Slowdown material | Aluminium | |
| Shielding beam blocker material | Vacuum | |

## 6.1 Simulation in the $^{17}$C Region

A number of simulations were conducted using nuclides in the neighborhood of $^{17}$C on the nuclide chart (see Figure 13). The value of $B\rho$ was calculated to $B\rho \approx 12.08\,\mathrm{Tm}$ for incident $^{17}$C ions that had an energy of 650 MeV/u. This was done using the *Sharp Calculator*, a special tool for calculating $B\rho$ values [6]. Using this $B\rho$ value, appropriate ion energies for the other ions in the vicinity of $^{17}$C in the nuclear chart were calculated.

Simulations were conducted with $2 \cdot 10^6$ incident ions, each of the ion species $^{16}$B, $^{16}$C, $^{16}$N, $^{17}$B, $^{17}$C, $^{17}$N, $^{18}$B, $^{18}$C and $^{18}$N using the detector standard settings (Table 2). The value of the effective degrader thickness was chosen using `ATIMA` and empirical studies, see section 5.2.1 for more information. The beam blocker thickness was chosen

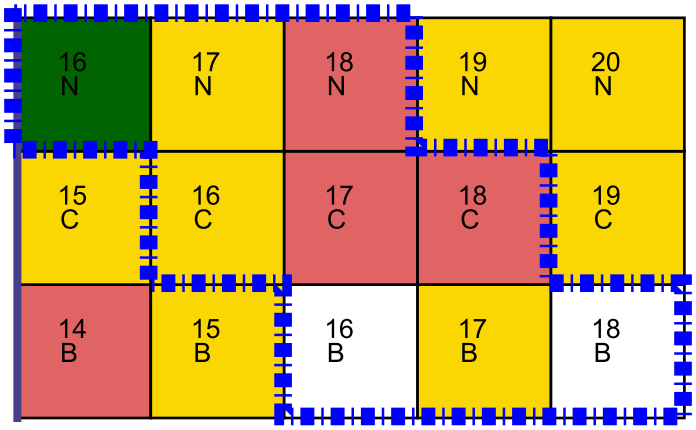


**Figure 13:** The nuclides inside the blue box are the ones simulated in the $^{17}$C region. Red nuclides are possibly identifiable with the PIBID detector and green by the ITAG detector.

by visually inspecting the detector under particle beam incidence, in order to find out a minimum possible thickness for the beam blocker.

The data from the simulations was mixed with the event mixer using a range of mixing times over several orders of magnitude. Thereafter the analysis program was run with the mixed data. Some different settings for the analysis were tested, such as allowing double implanted ions and waiting different times before allowing the next implantation. Statistics from the data analysis program was studied in order to draw conclusions about how the settings affected the quality of the identification. The all-event statistics were in the form of 24 dependent variables obtained during analysis. The most interesting variables is the number of coincidences, the number of correct coincidences and the intensity of the particles counted as number of fired particles per second. This intensity is not the same as the intensity of the incident beam, as all particles in the beam will not reach the sensitive parts of the detector. Neither the detector, event mixer or analysis software has any information about these "missed" events since they were not detected anywhere, and therefore the actual intensity of the incident beam is for our purposes an unknown parameter. Furthermore, to measure the intensity in number of events per second rather than number of fired particles per second per unit of detector area should more properly indicate at what conditions the detector can be operated, since the beam intensity can be changed (using beam blockers etc.) until the number of events are correct. The variables mentioned are plotted in Figure 14 for different analysis settings.

The conclusion from Figure 14 is that with increasing intensity, the number of identified coincidences for a run decreases. The time for a specific number of coincidences to be identified is not entirely clear from these figures, for that see Figure 15. As is clear from the plots in Figure 15 and 15, the acceptable amount of incorrect coincidences determines how high the intensity can become.

An identification plot is shown in figure 16. This will be similar to the output from the detector software run during a real-world experiment, and will help interpret the results. The reason for the missing $^{16}$B and $^{18}$B is that these isotopes are very unstable. $^{16}$B decays emitting a neutron with a half-life of less than 190 ps. At 80 % of light speed, as was the case here, this corresponds to about 10 cm travelled in the laboratory reference system. $^{18}$B decays with a half-life of 26 ns, which corresponds to about 13 m in the laboratory reference frame at 80 % of light speed.

Since the thickness of the wedges were adapted for $^{17}$C, this isotope shows the best spectra. $^{17}$C nuclei would stop in the middle of the scintillators (on average), while the other nuclei might on average stop more or less off of the middle. Also, only the isotopes $^{17}$C, $^{18}$C and $^{18}$N can be identified in the region in question, as the other isotopes there do not fulfill the identification conditions for the Precalibrated Ion Beam Identification Detector.. That is, the identifications of the other isotopes in the region will always be incorrect.

The peak at 1.15 MeV for fired $^{17}$C nuclides in Figure 16 is also a gamma line for $^{17}$C. However, it has a smaller probability, and is therefore disregarded by the analysis software.

Double implantation *not* allowed

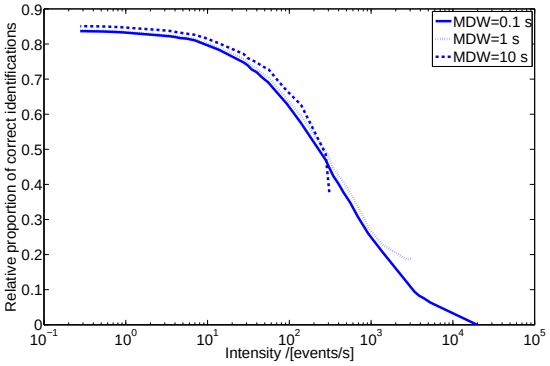


**(a)** Relative number of correct coincidences, as a function of the particle beam intensity. No double implantation allowed.

Double implantation allowed

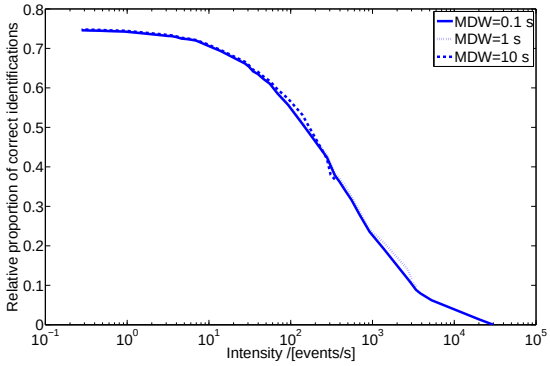


**(b)** Relative number of correct coincidences, as a function of the particle beam intensity. Double implantation allowed.

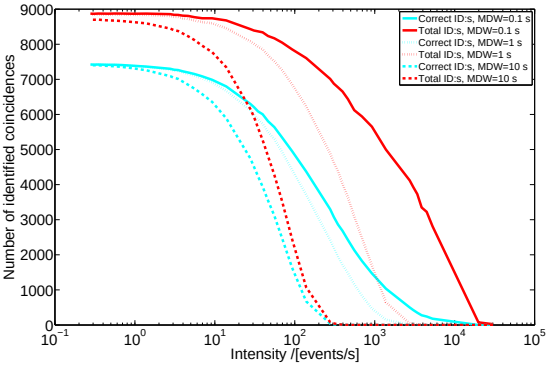


**(c)** Absolute number of coincidences (red) and absolute number of correct coincidences (cyan), as a function of the particle beam intensity. No double implantation allowed.

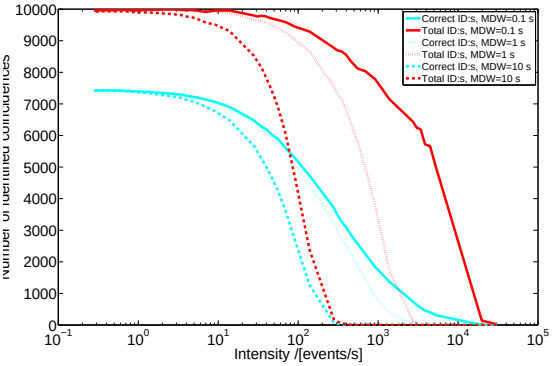


**(d)** Absolute number of coincidences (red) and absolute number of correct coincidences (cyan), as a function of the particle beam intensity. Double implantation allowed.

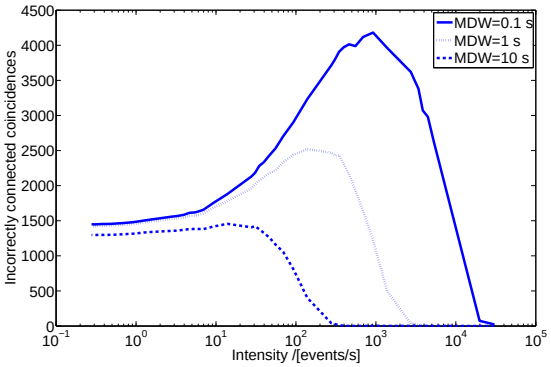


**(e)** Absolute number of incorrectly identified coincidences, not allowing double implantation, as a function of particle beam intensity.

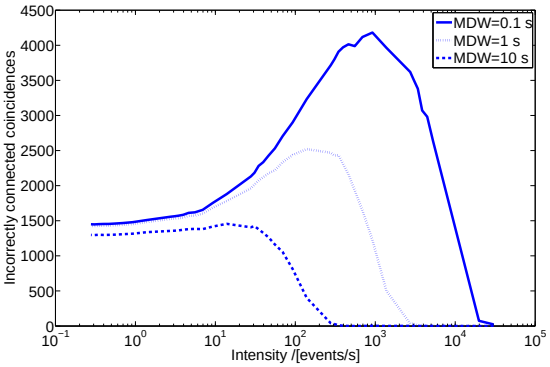


**(f)** Absolute number of incorrectly identified coincidences, when allowing double implantaion, as a function of particle beam intensity.

**Figure 14:** Coincidence correctness for $^{17}$C as function of particle beam intensity for different analysis settings. MDW means Maximum Decay Wait, as described in section 5.5.

Double implantation *not* allowed

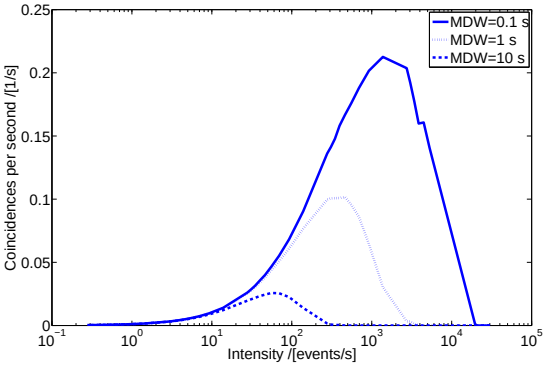


**(a)** Number of correct coincidences per second, as a function of the particle beam intensity. No double implantation allowed.

Double implantation allowed

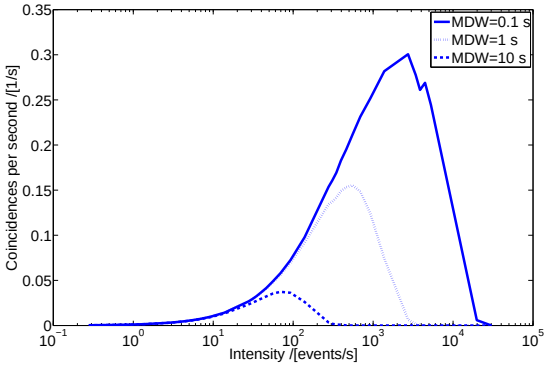


**(b)** Number of correct coincidences per second, as a function of the particle beam intensity. Double implantation allowed.

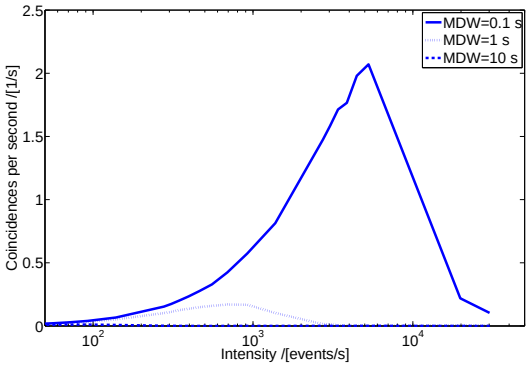


**(c)** Number of incorrect coincidences per second, as a function of the particle beam intensity. No double implantation allowed.

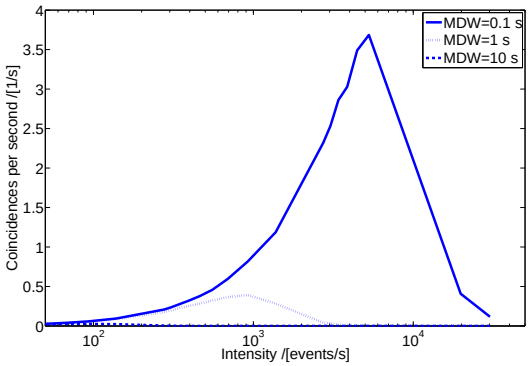


**(d)** Number of incorrect coincidences per second, as a function of the particle beam intensity. Double implantation allowed.

**Figure 15:** Coincidence correctness for $^{17}$C as function of particle beam intensity for different analysis settings. MDW means Maximum Decay Wait, as described in section 5.5.

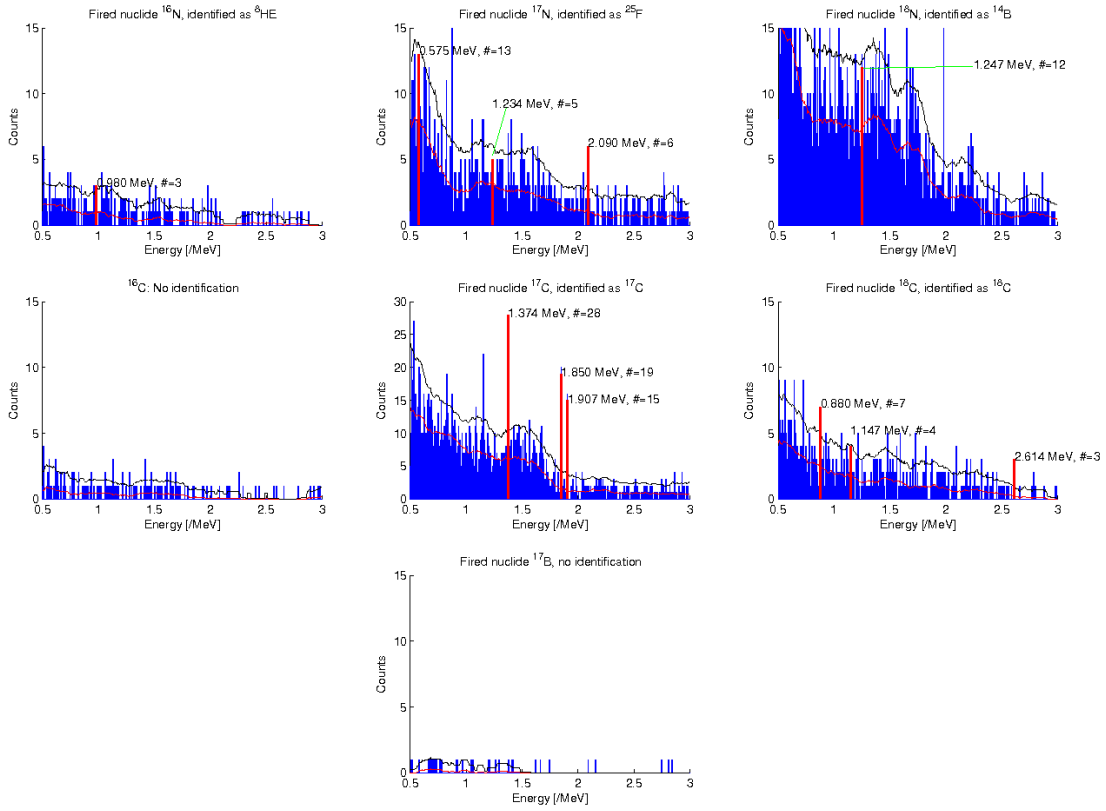


**Figure 16:** ID plot for $^{17}$C, using an intensity of 140 events per second for 13 hours and 27 minutes. This corresponds to $1{,}8 \cdot 10^7$ fired particles. The red line corresponds to a sliding average, and the black line corresponds to a sliding average plus two times the standard deviation. In creating the lines, the 10 % highest and the 10 % lowest values were discarded in order to prevent the peaks from affecting their vicinity.

## 6.2 Simulations Using Smaller Scintillator Tubes

Using the detector settings above, the intensity of the incoming ions must be relatively low in order to avoid double implantations which will confuse the identification process. However, this low intensity comes with a price: the detection takes longer time. While desirable detection times would be shorter than one hour, the identification above took over 13 h. Since number of incoming ions from the experiment can be taken as high as $10^5\,\mathrm{s}^{-1}$, a higher intensity could be used if the detector could handle it. This would be beneficial if it were possible to also increase the number of scintillator tubes, since the probability for simultaneous implantations would increase. The idea would be to decrease the scintillator sizes in order to allow for more scintillators in the same volume. In order to investigate this, simulations with $^{17}$C were run with different scintillator diameters. The scintillator diameter was set to values between 1 mm and 10 mm in steps of 1 mm. The other detector settings were the standard settings in Table 2.

Since the size of the scintillator tubes changed while distance between the scintillators and the surrounding shielding remained unchanged, the geometry of the detector was changed. The event mixer, however, kept the number of fired and detected particles per unit time approximately the same. Since, as seen in the direction of the beam, the scintillator tube and scintillator plate area were smaller relative the (constant) area of the beam blocker, the actual intensity of the incoming beam increases with decreasing scintillator tube. Therefore, fewer of the fired particles were detected. However, the relevant quantity should be the number of events per second, which gives an indication of how many particles went past the scintillator plates every second (and thus were availible for implantation). Not all events are implantations, but their numbers are in the same order of magnitude. The relative number of correct coincidences as a function of the tube diameter are depicted in Figure 17. The number of events per second was also approximate, and about 15 % lower for the smallest tube size compared to the largest. This was probably due to fewer detected decays with smaller tubes, as was to be expected.

As is clear from Figure 17, the accuracy of identification decreases as the scintillator tube diameter decreases. A deeper analysis of the raw simulation data indicated that this might be due to an increased number of implants in the scintillator shielding relative to the number of implants in the actual scintillators. Therefore, simply decreasing the scintillator diameter is not enough in order to utilize a higher intensity.

## 6.3 Simulations Using Thinner Shielding

In the same fashion as with the smaller scintillator tubes, smaller shielding might open up the possibility of having more scintillator tubes. Also, it might improve the quality of gamma radiation, in case it were that the shielding was absorbing or scattering some gamma photons. Therefore simulations were run using different shielding thickness. The top shielding thickness and shielding thickness was changed independently of each other from 10 mm to 2 mm in steps of 2 mm. The other simulation settings were as in Table 2.

The results of the shielding change were easy to evaluate by inspection of the his-

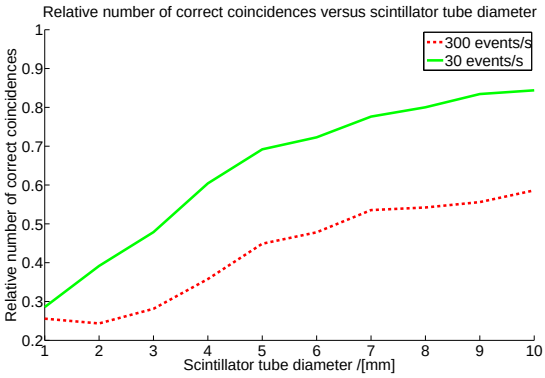


**Figure 17:** Relative number of correct coincidences as function of tube diameter. The number of events per second is approximate, and varies from about 15 % lower for the smallest scintillator tube size due to a decreased number of detected decays when the scintillator diameter becomes smaller. The average frequency of fired, detected particles is however the same for each curve. An alternative to holding the number of events per second fixed would be to fix the number of events per second per area unit.

togram delivered by the analysis software. The results turned out to be dependent on the number of events per second in the detector. For a top shielding thickness of 10 mm and shielding thickness of 10 mm a good spectrum could be obtained using both 3000 events/s and 300 events/s. For a shielding thickness of 2 mm and top shielding thickness of 2 mm, $^{17}$C could still be identified using 300 events/s although the intensity of the background noise was very high (probably due to electrons entering the Ge detector). However, using 3000 events/s identification was impossible.

## 6.4 Simulations Using a Different Shielding Material

Simulations with different shielding material between the scintillators were run using $^{17}$C. The materials quartz, iron and aluminium were tried, with the other settings taken as the standard settings in table 2. These materials were selected since they were likely to hinder electrons, but not gamma photons.

The results are displayed in Figure 18. As can be seen, quartz tend to block less than aluminium and iron, but in turn causes the relative coincidence correctness to be mentionable lower. Judging from Figure 18b, one should select aluminium or iron if one only cares about the high percentage of correct implantations. Using Figure 18a aluminium seems to give the best output among these alternatives.

## 6.5 Simulations Using a Shielding Beam Blocker

In order to decrease the number of implants in the shielding, a shielding beam blocker made of lead was deployed in front of the shielding material. This was an unstable measure, as it was a hindrance for ions entering the detector in a too large angle. It also

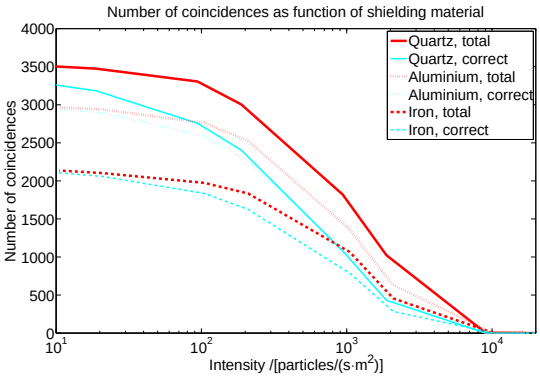


**(a)** Number of correctly identified coincidences and total number of coincidences for different materials in the shielding between the scintillators.

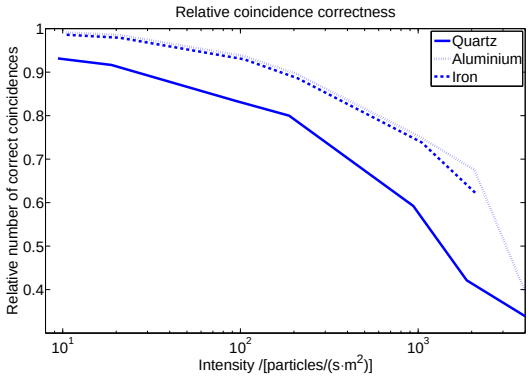


**(b)** Relative number of correctly identified coincidences for different materials in the shielding between the scintillators.

**Figure 18:** Correct and incorrect coincidences for different shielding materials.

prevented particles with high energy from passing through the shielding material and exiting. Simulations were run using $^{17}$C. The standard settings in table 2 were used, except from the shielding beam blocker size which was set to 2 cm, 5 cm, 10 cm and 15 cm, and the shielding beam blocker material which was taken as lead and vacuum.

The results of the simulations are shown in Table 3. The 15 cm shielding beam blocker thickness did barely generate any events, and was therefore omitted from the table. The reason for the low generation of events is likely reduced possible angular spread of the ion beam.

As is clear from table 3, the number of events decreased with about 25 % in all cases, while the number of correctly identified decays increased in some cases. The decrement in number of events is mostly due to a decreased number of decays, which is to be expected since there should be fewer implantations in the shielding beam blockers. The results of these simulations indicate that it would indeed be beneficial to add a shielding beam blocker, but that it would not need to be very thick. However, questions regarding this remain, as the shielding beam blocker might introduce unwanted effects using a mixture of isotopes and not only $^{17}$C. If so, it would probably be because those other isotopes might not have energies adapted for being stopped in the middle of the scintillators.

## 6.6 Simulations Using Different Ge Detector Radii

The Compton scattering in the Germanium detector is apparently high. It was therefore postulated that the Compton scattering might decrease if the radius of the Ge detector increased, so that a higher fraction of the photons would be photo absorbed before leaving the detector. Therefore, simulations were run using different radii of the Germanium detector, and the resulting spectra of coincidences were analyzed using visual inspection. The simulation settings were as in Table 2, with the exception of some parameters of

**Table 3:** Results of the simulations in section 6.5. The correctness and number of events are relative to the numbers obtained for a simulation without shielding beam blocker.

| **Thickness** | **Relative number of events** | **Relative number of decays** | **Relative number of implantations** | **Intensity** | **Relative correctness** |
|---|---|---|---|---|---|
| 2 cm | 77 % | 57 % | 100 % | 300 events/s | 111 % |
| | | | | 30 events/s | 105 % |
| | | | | 3 events/s | 103 % |
| 5 cm | 76 % | 53 % | 93 % | 300 events/s | 106 % |
| | | | | 30 events/s | 93 % |
| | | | | 3 events/s | 90 % |
| 10 cm | 75 % | 50 % | 88 % | 300 events/s | 110 % |
| | | | | 30 events/s | 94 % |
| | | | | 3 events/s | 89 % |

the Ge detector. Its radius was changed from 2.0 mm to 4.4 mm in steps of 0.3 mm. The inner radius of the germanium casing was always 0.3 mm greater than the radius of the germanium crystal, and the outer radius was always 0.6 mm greater.

The resulting identification plots are shown in Figure 19 for the extreme cases. As is clear from the figure, the background seems to be greater in proportion to the peaks for the larger radius. This might be due to more electrons and other particles hitting the Ge detector. Worth to bear in mind when observing the identification plots is that the total number of events for Figure 19b is about 20 % smaller than for Figure 19a. This is due to a changed geometry using the same number of fired particles.

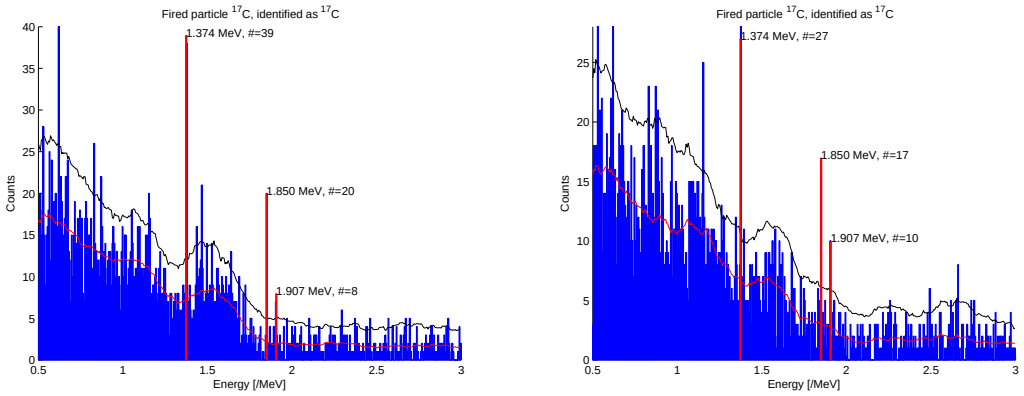


**(a)** Germanium crystal radius 2.0 mm. **(b)** Germanium crystal radius 4.4 mm.

**Figure 19:** Gamma spectrum for $^{17}$C for different radii of the germanium crystal. The radius of the casing was constant, as well as the distance between the casing and the crystal. The number of events was approximately 20 % higher for the smaller radius, due to a different detector area with the larger Ge detector.

# 7 Outlook and Conclusion

In this project a detector for identifying ions in particle beams has been investigated. The investigation was a many-step process, including the creation of a search program for the `ENSDF` nuclide database, identification of isotopes suitable for detection, simulations of the detector using the `Geant4` toolkit, and analysis of the simulated data.

While the evaluation of the detector design has given promising results, the design has not yet matched the time requirement of real experiments. In order for it to provide a practical advantage over existing methods, the detector would have to perform its task within approximately one hour. Currently the identification of $^{17}$C seems to take approximately 10 times as long. However, there is hope. Tweaking the detector design might optimize the detector to the point making it beneficial to build, something that future studies will have to look into.

Future studies will also have the advantage of using completed, well-documented software instead of writing everything from scratch. Some of the following topics might be interesting for such studies.

## 7.1 Improved detector design

The detector design has been evaluated with respect to some parameters. However, there might be other changes in the design that could drastically improve the detector performance. Another thing to study could be how another scintillator tube lengths would affect detector performance. Yet another could be optimizing the thickness of the casing of the germanium detector. A radically different geometry is also a possibility. This might include adding other detectors to obtain more data, or removing detectors to improve cost effectiveness. One rather different suggestion would be to replace the front scintillator plates with plates having small scintillating circles in front of each of the scintillators, in order to improve accuracy.

## 7.2 Improvements in detection algorithms

The detection algorithms used for the analysis are very simple. It is believed that better identification algorithms could be used for identifying the nuclides once the gamma energies are obtained from the coincidence conditions.

These algorithms might for instance use collected data to estimate the lifetimes of the nuclides, and then compare these estimations to the lifetimes listed in a database in order to check whether each identification made is reasonable.

# 8 References

[1] K. Larsson. *Forskargruppen Subatomär fysik*. Chalmers, 2006. http://www.chalmers.se/fp/SV/forskning/forskargrupper/subatomar-fysik1646. [Accessed 2012-02-05].

[2] R. Thies. *Prototype tests and pilot experiments for the* $R^3B$ *scintillator-based detection setup.* Master's thesis, Department of Fundamental Physics, Chalmers University of Technology, Gothenburg, 2011.

[3] F. Farinon. *ITAG Manual*, 2010. http://www-wnt.gsi.de/frs/technical/FRSsetup/detectors/itag/itag_manual.pdf. [Accessed 2012-02-05].

[4] H. T. Johansson. *The DAQ always runs - Performing large scale nuclear physics experiments*. Lic thesis, Department of Fundamental Physics, Chalmers University of Technology, Gothenburg, 2009.

[5] Geant4 official website. *Geant4: a toolkit for the simulation of the passage of particles through matter*. Geant4. http://geant4.cern.ch/. [Accessed 2012-05-13].

[6] Behr, K. H. and Geissel. *Sharp Calculator*. The FRS Setup. http://www-w2k.gsi.de/frs-Setup/Sharp%20Calculator.htm. [Accessed 2012-04-22].

[7] Brookhaven National Laboratry. *Evaluated Nuclear Structure Data File*. National Nuclear Data Center. http://www.nndc.bnl.gov/ensdf/. [Accessed 2012-04-21].

[8] H. Geissel, C. Scheidenberger, P. Malzacher, J. Kunzendorf, and H. Weick. *ATIMA*. GSI. http://www-linux.gsi.de/~weick/atima/. [Accessed 2012-04-23].

[9] Alian & ShiftB. *elog # 666*. GSI elog: Sat Sep 4 00:44:19 2010. http://elog.gsi.de/S393. [Image via Håkan Johansson. Requires login].

[10] Wikimedia Foundation. *Bethe formula*. Wikipedia. http://en.wikipedia.org/wiki/Bethe_formula. [Accessed 2012-04-24].

[11] Yuliya Aksyutina. *Light Unbound Nuclear Systems beyond the Dripline*. PhD thesis, Johann Wolfgang Goethe-Universität, Frankfurt am Main, 2009.

[12] Thomas I Nilsson. *K8 - Koincidensmätning*. Chalmers Tekniska högskola / Göteborgs Universitet, Fysiska Institutionen, 1994.

[13] *Chapter 8 Hyper-Pure Germanium Detector*. McMaster University. http://www.science.mcmaster.ca/medphys/images/ files/courses/4R06/note8.pdf. [Accessed 2012-04-20].

[14] Wikimedia Foundation. *Klein-Nishina formula*. Wikipedia. `http://en.wikipedia.org/wiki/Klein-Nishina_formula`. [Accessed 2012-04-21].

[15] B. R. Martin. *Nuclear and Particle Physics*. 2009.

[16] Paul James Mutton. *EpsGraphics2D*, 2004. `http://www.jibble.org/`. [Accessed 2011-07-20].

[17] P. Armbruster, et al. *Low-energy fission investigated in reactions of 750 AMeV 238U-ions with Pb and Be targets. Zeitschrift für Physik A Hadrons and Nuclei*, 355:191–201, 1996.

[18] S. Pietri, P.H. Regan, Zs. Podolyák, D. Rudolph, S. Steer, A.B. Garnsworthy, E. Werner-Malento, R. Hoischen, M. Górska, J. Gerl, H.J. Wollersheim, I. Kojouharov, H. Schaffner, F. Becker, P. Bednarczyk, L. Caceres, P. Doornenbal, H. Geissel, J. Grębosz, A. Kelic, N. Kurz, F. Montes, W. Prokopowicz, T. Saito, S. Tashenov, A. Heinz, M. Pfützner, T. Kurtukian-Nieto, G. Benzoni, M. Hellström, A. Jungclaus, J. Simpson, L.-L. Andersson, L. Atanasova, D. Balabanski, M.A. Bentley, B. Blank, A. Blazhev, C. Brandau, J.R. Brown, A.M. Bruce, F. Camera, W.N. Catford, I.J. Cullen, Zs. Dombrádi, E. Estevez, C. Fahlander, W. Gelletly, G. Ilie, E.K. Johansson, J. Jolie, G.A. Jones, M. Kmiecik, F.G. Kondev, S. Lalkovski, Z. Liu, A. Maj, S. Myalski, T. Shizuma, A.J. Simons, S. Schwertel, P.M. Walker, and O. Wieland. *Recent results in fragmentation isomer spectroscopy with rising. Nuclear Instruments and Methods in Physics Research Section B: Beam Interactions with Materials and Atoms*, 261(1–2):1079 – 1083, 2007. The Application of Accelerators in Research and Industry - Proceedings of the Nineteenth International Conference on The Application of Accelerators in Research and Industry.

[19] F. Humbert, T. Nilsson, W. Schwab, M. Zinser, Th. Blaich, M.J.G. Borge, L.V. Chulkov, Th.W. Elze, H. Emling, B. Franzke, H. Freiesleben, H. Geissel, K. Grimm, D. Guillemaud-Mueller, P.G. Hansen, R. Holzmann, H. Irnich, L. Johannsen, B. Jonson, J.G. Keller, O. Klepper, H. Klingler, J.V. Kratz, R. Kulessa, D. Lambrecht, Y. Leifels, A. Magel, M. Mohar, A.C. Mueller, G. Münzenberg, P. Møller, F. Nickel, G. Nyman, A. Richter, K. Riisager, C. Scheidenberger, G. Schrieder, B.M. Sherrill, H. Simon, K. Stelzer, J. Stroth, O. Tengblad, W. Trautmann, E. Wajda, and E. Zude. *Longitudinal and transverse momentum distributions of 9Li fragments from break-up of 11Li. Physics Letters B*, 347(3–4):198 – 204, 1995.

## Personal Communication

[20] H. T. Johansson. (2011-08-08) Discussion with R. Lundmark.

[21] H. T. Johansson. (2012-02-05) Personal mail to R. Lundmark (riklund@student.chalmers.se).

[22] H. T. Johansson. (2012-04-24) Discussion with R. Lundmark and P. Collet.

[23] J. Tuli. (2011-06-23 – 2011-07-01) Personal mail to R. Lundmark (riklund@student.chalmers.se).

[24] Stefan Isaksson. Gammadata Instruments. (2012-04-24) Personal mail to R. Lundmark (riklund@student.chalmers.se).

# 9 Glossary

**Active detector part** Part of the detector that can detect particles, for example scintillator tubes or germanium detector.

**B$\rho$-value** Product of magnetic field ($B$) and radius of curvature ($\rho$) in a mass spectrometer. For a specific particle type (mass and charge) this implies a specific velocity is required to pass.

**ENSDF** Evaluated Nuclear Structure Data File. A database containing evaluated nuclear structure and decay information for over 3000 nuclides [7].

**ENSDF++** Search program for the `ENSDF` database. See Appendix A.1 for more information.

**Event** An event is the measured energies in all detectors, summed over a specific time frame. In the simulations in this project, this summation time was 1 $\mu$s.

**FRS** FRagment Separator.

**EventMixer** Program for mixing events generated by the PIBIDS software. See Appendix A.2 for more information.

**"Ion" versus "particle"** All particles in the experimental context of the proposed detector will be completely stripped of electrons, and thus be ions. In this thesis the words "particle" and "ion" are therefore used interchangeably.

**ITAG** Isomer TAgging Detector. Detector for identifying isomers used at GSI. See Section 3.3.2 for more information.

**MDW** Maximum Decay Wait time. The maximum time that the MDCAS software will wait between an implantation and a decay before it marks the scintillator tube in which the implantation occurred as availible for a new implantation.

**MDCAS** Mixed Data Coincidence Analysis Software. The data analysis tool used for analysing the output from PIBIDS. See Appendix A.5 for more information.

**Passive detector part** Part of the detector that is not an active part.

**PIBID** Precalibrated Ion Beam Identification Detector. The name of the detector this project is evaluating. Also the name of the thesis.

**PIBIDS** Precalibrated Ion Beam Identification Detector Simulation. The detector simulation. See Appendix A.2 for more information.

**RootMaker** Program for making root files of the output from the PIBIDS software. See Appendix A.4 for more information.

# A Additional Material

The source code from this project can be found at different sub-pages to `http://fy.chalmers.se/subatom/kand/2012/precalib/`.

## A.1 ENSDF++

Documentation and downloadable source code for the ENSDF++ software can be found at `http://fy.chalmers.se/subatom/kand/2012/precalib/ENSDF++`. This page contains all information needed to set up the search program and implement customized search queries.

## A.2 PIBIDS

Documentation and downloadable source code for the Precalibrated Ion Beam Identification Detector Software can be found at `http://fy.chalmers.se/subatom/kand/2012/precalib/PIBIDS`. In addition to the source code obtained from this web page, a local installation of `Geant4` with the additional PhotonEvaporation data must be set up. The output data format from the software is also specified here.

## A.3 EventMixer

The source code and documentation for the EventMixer software can be found at `http://fy.chalmers.se/subatom/kand/2012/precalib/EventMixer`.

## A.4 RootMaker

The source code and documentation for the RootMaker software can be found at `http://fy.chalmers.se/subatom/kand/2012/precalib/RootMaker`.

## A.5 MDCAS

The source code and documentation for the Mixed Data Coincidence Analysis Software software can be found at `http://fy.chalmers.se/subatom/kand/2012/precalib/MDCAS`. The source code from this web page is everything required to do coincidence analysis using data from the event mixing software.

# B Identifiable Nuclides

The following list of nuclides identifiable by the Precalibrated Ion Beam Identification Detector has been generated using the `ENSDF++`-software. The criteria for the gamma energies shown are that they have a probability of $\geq 10\,\%$ of being emitted for each implanted ion. The criteria on the isotopes shown are also a half-life of between 1 ms and 1 s. Short half-lives are advantageous as they reduce the probability of double implantation. In a few cases the probabilities are greater than 100 %. The reason for this has been investigated, and the explanation is that the total beta decay probability given in the database is greater than 100 %. The reason for this is thought to be experimental error. ENSDF is after all a database containing experimental data, not theoretical. This decay probability might propagate through the gamma decay computations and give a gamma probability much greater than 100 % if the beta probability is only a few percent off.

**Table 4:** Gamma lines of identifiable isotopes.

| Isotope | Half-life | Gamma energies | Emission probability |
|---|---|---|---|
| $^{8}$He | 119 ms | 980.0 keV | 98 % |
| $^{14}$B | 12 ms | 6093.8 keV | 92 % |
| | | 6728.2 keV | 11 % |
| $^{17}$C | 193 ms | 1373.9 keV | 18 % |
| | | 1849.6 keV | 17 % |
| | | 1906.8 keV | 10 % |
| $^{18}$C | 92 ms | 114.9 keV | 31 % |
| | | 879.6 keV | 15 % |
| | | 2499.6 keV | 13 % |
| | | 2614.5 keV | 29 % |
| $^{18}$N | 624 ms | 821.8 keV | 38 % |
| | | 1651.7 keV | 39 % |
| | | 1982.1 keV | 65 % |
| | | 2424.9 keV | 10 % |
| | | 2473.5 keV | 13 % |
| $^{24}$O | 65 ms | 1831.3 keV | 11 % |
| $^{25}$F | 80 ms | 574.8 keV | 11 % |
| | | 1613.6 keV | 16 % |

Continued on next page

**Table 4 – continued from previous page**

| Isotope | Half-life | Gamma energies | Emission probability |
|---|---|---|---|
| | | 1702.8 keV | 47 % |
| | | 2090.0 keV | 14 % |
| $^{26}$F | 10 ms | 1673.0 keV | 17 % |
| | | 2018.3 keV | 61 % |
| $^{25}$Ne | 602 ms | 89.5 keV | 95 % |
| | | 979.8 keV | 18 % |
| $^{27}$Ne | 32 ms | 63.0 keV | 21 % |
| $^{28}$Ne | 19 ms | 55.0 keV | 27 % |
| | | 2063.1 keV | 17 % |
| $^{30}$Ne | 7 ms | 150.6 keV | 68 % |
| $^{20}$Na | 448 ms | 1633.7 keV | 99 % |
| | | 1633.7 keV | 82 % |
| | | 5788.2 keV | 16 % |
| $^{27}$Na | 301 ms | 984.7 keV | 86 % |
| | | 1698.0 keV | 11 % |
| $^{28}$Na | 30 ms | 1474.0 keV | 37 % |
| | | 2389.2 keV | 19 % |
| $^{29}$Na | 45 ms | 54.6 keV | 32 % |
| | | 2560.3 keV | 28 % |
| $^{30}$Na | 48 ms | 1482.5 keV | 31 % |
| $^{32}$Na | 13 ms | 885.5 keV | 46 % |
| | | 2151.4 keV | 25 % |
| $^{21}$Mg | 122 ms | 331.9 keV | 50 % |
| $^{30}$Mg | 335 ms | 244.1 keV | 55 % |
| | | 443.9 keV | 53 % |
| $^{31}$Mg | 230 ms | 666.3 keV | 15 % |
| | | 946.5 keV | 42 % |
| | | 1612.8 keV | 45 % |
| | | 1626.2 keV | 28 % |
| $^{32}$Mg | 86 ms | 2765.3 keV | 21 % |

Continued on next page

**Table 4 – continued from previous page**

| Isotope | Half-life | Gamma energies | Emission probability |
|---|---|---|---|
| $^{23}$Al | 470 ms | 450.7 keV | 54 % |
| $^{24}$Al | 131 ms | 1368.7 keV | 29 % |
| $^{31}$Al | 644 ms | 1695.0 keV | 11 % |
| | | 2316.8 keV | 19 % |
| $^{32}$Al | 33 ms | 1941.4 keV | 12 % |
| $^{34}$Al | 42 ms | 125.4 keV | 23 % |
| | | 929.6 keV | 51 % |
| | | 3327.7 keV | 61 % |
| | | 4257.3 keV | 11 % |
| $^{25}$Si | 220 ms | 452.0 keV | 16 % |
| | | 493.0 keV | 16 % |
| | | 945.0 keV | 11 % |
| | | 1613.0 keV | 15 % |
| $^{35}$Si | 780 ms | 241.3 keV | 31 % |
| | | 392.4 keV | 16 % |
| | | 2386.4 keV | 22 % |
| | | 3859.7 keV | 40 % |
| | | 4101.0 keV | 42 % |
| $^{36}$Si | 450 ms | 175.0 keV | 71 % |
| | | 249.9 keV | 73 % |
| | | 424.9 keV | 33 % |
| | | 878.2 keV | 44 % |
| | | 921.4 keV | 16 % |
| | | 934.7 keV | 13 % |
| | | 1856.1 keV | 28 % |
| $^{28}$P | 270 ms | 1779.0 keV | 97 % |
| | | 4497.5 keV | 11 % |
| $^{38}$P | 640 ms | 1292.3 keV | 70 % |
| | | 2224.2 keV | 16 % |
| $^{29}$S | 187 ms | 1383.6 keV | 45 % |

Continued on next page

**Table 4 – continued from previous page**

| Isotope | Half-life | Gamma energies | Emission probability |
|---|---|---|---|
| | | 1953.9 keV | 18 % |
| | | 2422.7 keV | 23 % |
| $^{32}$Cl | 298 ms | 2230.3 keV | 94 % |
| | | 4772.2 keV | 21 % |
| $^{32}$Ar | 98 ms | 89.9 keV | 12 % |
| | | 466.1 keV | 12 % |
| | | 702.4 keV | 12 % |
| | | 1078.6 keV | 12 % |
| | | 1168.5 keV | 32 % |
| $^{35}$K | 178 ms | 1750.6 keV | 14 % |
| | | 2589.9 keV | 26 % |
| | | 2982.8 keV | 50 % |
| $^{36}$K | 342 ms | 1970.4 keV | 82 % |
| | | 2207.9 keV | 30 % |
| | | 2432.9 keV | 31 % |
| $^{51}$K | 365 ms | 3462.0 keV | 11 % |
| $^{53}$K | 30 ms | 2200.0 keV | 15 % |
| $^{36}$Ca | 102 ms | 1112.8 keV | 13 % |
| | | 1619.0 keV | 30 % |
| $^{38}$Ca | 440 ms | 1567.8 keV | 20 % |
| $^{40}$Sc | 182 ms | 754.8 keV | 40 % |
| | | 1122.5 keV | 11 % |
| | | 1877.3 keV | 24 % |
| | | 2045.2 keV | 24 % |
| | | 3167.7 keV | 11 % |
| | | 3735.8 keV | 97 % |
| | | 3922.5 keV | 12 % |
| $^{50}$Sc | 350 ms | 1553.8 keV | 100 % |
| | | 1553.8 keV | 100 % |
| $^{54}$Sc | 292 ms | 1001.2 keV | 55 % |

Continued on next page

**Table 4 – continued from previous page**

| Isotope | Half-life | Gamma energies | Emission probability |
|---|---|---|---|
| | | 1021.0 keV | 15 % |
| | | 1494.8 keV | 75 % |
| $^{42}$Ti | 199 ms | 611.1 keV | 56 % |
| $^{57}$Ti | 98 ms | 61.6 keV | 11 % |
| | | 113.2 keV | 14 % |
| | | 174.8 keV | 31 % |
| | | 1579.5 keV | 16 % |
| | | 1861.5 keV | 14 % |
| $^{44}$V | 150 ms | 1083.0 keV | 100 % |
| | | 1083.1 keV | 90 % |
| | | 1371.3 keV | 100 % |
| | | 1447.9 keV | 22 % |
| | | 1561.0 keV | 91 % |
| | | 2834.5 keV | 35 % |
| | | 3032.2 keV | 15 % |
| | | 5523.3 keV | 22 % |
| $^{57}$V | 350 ms | 267.9 keV | 52 % |
| | | 692.3 keV | 20 % |
| $^{61}$Cr | 243 ms | 354.9 keV | 16 % |
| | | 1142.3 keV | 21 % |
| | | 1860.8 keV | 20 % |
| | | 2378.2 keV | 11 % |
| $^{62}$Cr | 206 ms | 285.0 keV | 18 % |
| | | 285.0 keV | 18 % |
| | | 355.0 keV | 15 % |
| | | 355.0 keV | 15 % |
| | | 640.0 keV | 10 % |
| | | 640.0 keV | 10 % |
| $^{48}$Mn | 158 ms | 752.1 keV | 83 % |
| | | 1106.1 keV | 37 % |

Continued on next page

**Table 4 – continued from previous page**

| Isotope | Half-life | Gamma energies | Emission probability |
|---|---|---|---|
| | | 1364.0 keV | 20 % |
| | | 3676.4 keV | 28 % |
| | | 3934.3 keV | 21 % |
| $^{61}$Mn | 670 ms | 628.7 keV | 17 % |
| $^{62}$Mn | 671 ms | 877.3 keV | 116 % |
| | | 877.3 keV | 116 % |
| | | 941.9 keV | 22 % |
| | | 941.9 keV | 22 % |
| | | 1139.7 keV | 37 % |
| | | 1139.7 keV | 37 % |
| | | 1299.2 keV | 40 % |
| | | 1299.2 keV | 40 % |
| | | 1457.0 keV | 17 % |
| | | 1457.0 keV | 17 % |
| | | 1814.3 keV | 33 % |
| | | 1814.3 keV | 33 % |
| $^{64}$Mn | 90 ms | 746.6 keV | 35 % |
| $^{65}$Fe | 810 ms | 340.1 keV | 29 % |
| | | 736.2 keV | 13 % |
| | | 882.5 keV | 63 % |
| | | 1222.6 keV | 14 % |
| | | 1996.3 keV | 27 % |
| $^{64}$Co | 300 ms | 1346.1 keV | 10 % |
| $^{67}$Co | 425 ms | 694.1 keV | 94 % |
| $^{68}$Co | 199 ms | 271.9 keV | 45 % |
| | | 323.5 keV | 40 % |
| | | 595.4 keV | 33 % |
| | | 708.9 keV | 22 % |
| | | 815.0 keV | 111 % |
| | | 2033.2 keV | 111 % |

Continued on next page

**Table 4 – continued from previous page**

| Isotope | Half-life | Gamma energies | Emission probability |
|---|---|---|---|
| $^{58}$Zn | 86 ms | 203.0 keV | 82 % |
| | | 848.0 keV | 10 % |
| $^{79}$Zn | 995 ms | 278.7 keV | 11 % |
| | | 702.2 keV | 33 % |
| | | 707.6 keV | 11 % |
| | | 865.8 keV | 24 % |
| | | 874.6 keV | 14 % |
| | | 979.3 keV | 13 % |
| $^{80}$Zn | 540 ms | 642.2 keV | 14 % |
| | | 685.6 keV | 15 % |
| | | 712.5 keV | 45 % |
| | | 715.4 keV | 34 % |
| | | 965.0 keV | 15 % |
| | | 1151.2 keV | 13 % |
| $^{60}$Ga | 70 ms | 1003.7 keV | 89 % |
| | | 1555.0 keV | 11 % |
| | | 2558.7 keV | 11 % |
| | | 3848.2 keV | 51 % |
| $^{84}$Ga | 85 ms | 624.3 keV | 100 % |
| | | 1046.1 keV | 90 % |
| $^{92}$Br | 343 ms | 769.1 keV | 39 % |
| $^{71}$Kr | 100 ms | 198.0 keV | 15 % |
| | | 198.0 keV | 15 % |
| $^{94}$Kr | 212 ms | 219.3 keV | 17 % |
| | | 629.3 keV | 21 % |
| | | 764.5 keV | 15 % |
| $^{95}$Rb | 378 ms | 204.1 keV | 13 % |
| | | 204.1 keV | 13 % |
| | | 352.0 keV | 39 % |
| | | 352.0 keV | 39 % |

Continued on next page

**Table 4 – continued from previous page**

| Isotope | Half-life | Gamma energies | Emission probability |
|---|---|---|---|
| | | 680.7 keV | 12 % |
| | | 680.7 keV | 12 % |
| $^{96}$Rb | 203 ms | 814.9 keV | 69 % |
| $^{98}$Rb | 114 ms | 71.1 keV | 17 % |
| | | 144.2 keV | 100 % |
| | | 144.2 keV | 53 % |
| | | 289.3 keV | 25 % |
| | | 1693.3 keV | 14 % |
| | | 2171.6 keV | 15 % |
| $^{100}$Rb | 51 ms | 129.2 keV | 69 % |
| | | 287.8 keV | 21 % |
| | | 1201.7 keV | 11 % |
| $^{101}$Rb | 32 ms | 111.6 keV | 20 % |
| | | 251.6 keV | 20 % |
| | | 271.1 keV | 63 % |
| | | 1091.8 keV | 16 % |
| $^{97}$Sr | 429 ms | 652.0 keV | 10 % |
| | | 667.5 keV | 12 % |
| | | 953.8 keV | 21 % |
| | | 1904.9 keV | 22 % |
| $^{98}$Sr | 653 ms | 36.2 keV | 21 % |
| | | 119.4 keV | 81 % |
| | | 428.4 keV | 28 % |
| | | 444.6 keV | 24 % |
| | | 480.9 keV | 16 % |
| $^{99}$Sr | 270 ms | 125.1 keV | 18 % |
| | | 125.1 keV | 18 % |
| | | 536.2 keV | 13 % |
| | | 536.2 keV | 13 % |
| $^{100}$Sr | 202 ms | 10.7 keV | 115 % |

Continued on next page

**Table 4 – continued from previous page**

| Isotope | Half-life | Gamma energies | Emission probability |
|---|---|---|---|
| | | 65.4 keV | 31 % |
| | | 898.5 keV | 22 % |
| | | 963.9 keV | 25 % |
| $^{101}$Sr | 118 ms | 128.3 keV | 13 % |
| $^{102}$Sr | 69 ms | 67.8 keV | 10 % |
| | | 93.8 keV | 31 % |
| | | 150.1 keV | 18 % |
| | | 243.9 keV | 54 % |
| | | 254.0 keV | 12 % |
| $^{97}$Y | 142 ms | 161.4 keV | 71 % |
| | | 361.2 keV | 39 % |
| | | 407.2 keV | 29 % |
| | | 456.8 keV | 38 % |
| | | 456.8 keV | 39 % |
| | | 698.2 keV | 100 % |
| | | 817.9 keV | 61 % |
| | | 840.1 keV | 100 % |
| | | 949.6 keV | 56 % |
| | | 986.1 keV | 44 % |
| | | 999.5 keV | 62 % |
| | | 1103.1 keV | 76 % |
| | | 1400.1 keV | 24 % |
| $^{98}$Y | 548 ms | 1222.9 keV | 37 % |
| | | 1590.8 keV | 15 % |
| | | 2941.8 keV | 17 % |
| $^{100}$Y | 940 ms | 118.6 keV | 11 % |
| | | 118.6 keV | 37 % |
| | | 212.5 keV | 96 % |
| | | 212.5 keV | 89 % |
| | | 352.0 keV | 28 % |

Continued on next page

**Table 4 – continued from previous page**

| Isotope | Half-life | Gamma energies | Emission probability |
|---|---|---|---|
| | | 665.7 keV | 10 % |
| $^{108}$Nb | 193 ms | 192.9 keV | 87 % |
| | | 370.9 keV | 13 % |
| | | 393.2 keV | 20 % |
| | | 586.1 keV | 13 % |
| | | 590.2 keV | 41 % |
| $^{110}$Mo | 300 ms | 39.5 keV | 15 % |
| | | 53.3 keV | 24 % |
| | | 120.8 keV | 25 % |
| | | 142.1 keV | 50 % |
| | | 223.4 keV | 15 % |
| | | 598.7 keV | 10 % |
| $^{111}$Tc | 290 ms | 150.3 keV | 34 % |
| | | 150.3 keV | 34 % |
| | | 279.7 keV | 13 % |
| | | 279.7 keV | 13 % |
| | | 368.8 keV | 34 % |
| | | 368.8 keV | 34 % |
| $^{113}$Tc | 160 ms | 98.3 keV | 48 % |
| | | 164.1 keV | 26 % |
| | | 294.9 keV | 12 % |
| | | 335.3 keV | 16 % |
| | | 433.6 keV | 14 % |
| | | 1520.1 keV | 12 % |
| $^{113}$Ru | 800 ms | 88.1 keV | 14 % |
| | | 211.7 keV | 45 % |
| | | 227.6 keV | 11 % |
| | | 232.4 keV | 10 % |
| | | 263.1 keV | 30 % |
| | | 263.2 keV | 98 % |

Continued on next page

**Table 4 – continued from previous page**

| Isotope | Half-life | Gamma energies | Emission probability |
|---|---|---|---|
| | | 337.4 keV | 12 % |
| | | 337.5 keV | 16 % |
| | | 351.3 keV | 13 % |
| | | 1973.5 keV | 11 % |
| $^{114}$Ru | 530 ms | 52.7 keV | 15 % |
| | | 127.0 keV | 30 % |
| | | 128.2 keV | 15 % |
| | | 179.7 keV | 17 % |
| $^{116}$Rh | 570 ms | 328.4 keV | 16 % |
| | | 340.2 keV | 45 % |
| | | 340.3 keV | 85 % |
| | | 397.6 keV | 16 % |
| | | 397.6 keV | 15 % |
| | | 466.1 keV | 11 % |
| | | 537.3 keV | 46 % |
| | | 638.6 keV | 17 % |
| | | 681.4 keV | 14 % |
| | | 726.0 keV | 23 % |
| | | 737.8 keV | 11 % |
| | | 743.7 keV | 22 % |
| | | 1104.8 keV | 20 % |
| $^{120}$Ag | 320 ms | 505.9 keV | 32 % |
| | | 697.8 keV | 32 % |
| | | 925.8 keV | 23 % |
| $^{121}$Ag | 780 ms | 314.5 keV | 33 % |
| | | 353.5 keV | 20 % |
| $^{122}$Ag | 529 ms | 569.5 keV | 96 % |
| | | 650.2 keV | 20 % |
| | | 759.7 keV | 33 % |
| | | 798.3 keV | 13 % |

Continued on next page

**Table 4 – continued from previous page**

| Isotope | Half-life | Gamma energies | Emission probability |
|---|---|---|---|
| $^{123}$Ag | 300 ms | 263.9 keV | 39 % |
| | | 409.8 keV | 14 % |
| $^{125}$Cd | 680 ms | 436.3 keV | 47 % |
| | | 436.3 keV | 47 % |
| | | 1099.5 keV | 26 % |
| | | 1099.5 keV | 26 % |
| | | 1701.0 keV | 13 % |
| | | 1701.0 keV | 13 % |
| | | 2147.2 keV | 23 % |
| | | 2147.2 keV | 23 % |
| $^{128}$Cd | 340 ms | 68.0 keV | 105 % |
| | | 247.9 keV | 144 % |
| | | 857.0 keV | 90 % |
| | | 925.0 keV | 12 % |
| | | 1172.9 keV | 10 % |
| $^{130}$Cd | 162 ms | 451.0 keV | 42 % |
| | | 949.9 keV | 10 % |
| | | 1170.3 keV | 11 % |
| | | 1669.2 keV | 47 % |
| $^{128}$In | 720 ms | 91.1 keV | 90 % |
| | | 91.1 keV | 90 % |
| | | 120.6 keV | 14 % |
| | | 120.6 keV | 14 % |
| | | 321.2 keV | 11 % |
| | | 321.2 keV | 11 % |
| | | 831.5 keV | 104 % |
| | | 831.5 keV | 104 % |
| | | 1168.8 keV | 104 % |
| | | 1168.8 keV | 104 % |
| | | 1168.8 keV | 50 % |

Continued on next page

**Table 4 – continued from previous page**

| Isotope | Half-life | Gamma energies | Emission probability |
|---|---|---|---|
| | | 1867.1 keV | 33 % |
| | | 1867.1 keV | 33 % |
| | | 1973.9 keV | 20 % |
| | | 1973.9 keV | 20 % |
| | | 3519.9 keV | 17 % |
| | | 4297.7 keV | 12 % |
| $^{129}$In | 610 ms | 769.3 keV | 10 % |
| | | 1865.0 keV | 32 % |
| | | 2118.0 keV | 45 % |
| $^{130}$In | 290 ms | 89.2 keV | 54 % |
| | | 89.2 keV | 28 % |
| | | 96.5 keV | 12 % |
| | | 129.8 keV | 82 % |
| | | 129.8 keV | 11 % |
| | | 138.0 keV | 27 % |
| | | 138.0 keV | 14 % |
| | | 391.4 keV | 14 % |
| | | 774.3 keV | 57 % |
| | | 774.4 keV | 50 % |
| | | 952.6 keV | 12 % |
| | | 1221.3 keV | 78 % |
| | | 1221.3 keV | 75 % |
| | | 1905.2 keV | 79 % |
| | | 2028.3 keV | 11 % |
| | | 2258.9 keV | 90 % |
| | | 2377.2 keV | 17 % |
| $^{131}$In | 320 ms | 158.6 keV | 37 % |
| | | 173.2 keV | 43 % |
| | | 284.6 keV | 40 % |
| | | 2095.8 keV | 24 % |

Continued on next page

**Table 4 – continued from previous page**

| Isotope | Half-life | Gamma energies | Emission probability |
|---|---|---|---|
| | | 2380.4 keV | 16 % |
| | | 2434.2 keV | 105 % |
| | | 4102.1 keV | 11 % |
| | | 4273.3 keV | 105 % |
| $^{132}$In | 207 ms | 132.6 keV | 22 % |
| | | 299.6 keV | 48 % |
| | | 375.1 keV | 59 % |
| | | 479.0 keV | 25 % |
| | | 526.2 keV | 20 % |
| | | 2268.6 keV | 16 % |
| | | 2380.2 keV | 24 % |
| | | 4041.2 keV | 62 % |
| | | 4351.9 keV | 26 % |
| $^{135}$Sn | 530 ms | 281.8 keV | 18 % |
| $^{136}$Sb | 923 ms | 606.6 keV | 15 % |
| $^{140}$I | 860 ms | 376.7 keV | 101 % |
| | | 457.6 keV | 69 % |
| | | 937.4 keV | 19 % |
| $^{145}$Cs | 587 ms | 112.6 keV | 14 % |
| | | 175.3 keV | 21 % |
| | | 198.7 keV | 13 % |
| $^{147}$Ba | 894 ms | 74.5 keV | 20 % |
| | | 105.1 keV | 15 % |
| | | 167.4 keV | 17 % |
| $^{148}$Ba | 612 ms | 56.0 keV | 29 % |
| $^{149}$Dy | 490 ms | 290.6 keV | 18 % |
| | | 361.0 keV | 18 % |
| | | 559.6 keV | 18 % |
| | | 630.4 keV | 18 % |
| | | 786.5 keV | 18 % |

Continued on next page

**Table 4 – continued from previous page**

| Isotope | Half-life | Gamma energies | Emission probability |
|---|---|---|---|
| $^{152}$Lu | 700 ms | 312.6 keV | 66 % |
| | | 358.7 keV | 66 % |
| | | 1531.4 keV | 66 % |

# C Sammanfattning

Vid genomförande av experiment med radioaktiva strålar är det ett återkommande problem att identifiera de joner som förekommer. För identifikationen används olika detektorer, som före användning måste kalibreras — ofta med tillgång till stråle. Detta kandidatprojekt utvärderar ett koncept för en hjälpdetektor som kan kalibreras utan stråle. Den förkalibrerade detektorn används vid initialkalibreringen av övriga detektorer i experimentuppställningen, och kan därigenom spara dyr stråltid. Kalibreringen i fråga genomförs genom att absoluta identifikationer görs av individuella joner som detekterats av huvudexperimentuppställningen. I identifikationsprocessen utnyttjas koincidens mellan $\beta$- och $\gamma$-sönderfall.

## C.1 Bakgrund

Vid experiment med radioaktiva strålar, separerade av en magnetisk spektrometer (så kallad fragmentseparator), är det ett ständigt gissel att snabbt, enkelt och säkert identifiera de olika joner som passerar strållinjen. De detektorer som används behöver kalibreras för att leverera absolut information och detta kräver i sin tur att de beskjuts med joner av känd typ (laddning, massa) samt hastighet [22]. Det är därför av intresse att använda (hjälp-)detektorer som kan kalibreras utan stråle för att underlätta absolutkalibreringen och identifikationen.

### C.1.1 GSI

GSI Helmholtz Centre for Heavy Ion Research GmbH (GSI) är en acceleratorbaserad anläggning i Tyskland för forskning på tunga joner, som Chalmers avdelning för subatomär fysik har ett långvarigt samarbete med [1]. Avsikten är att den detektordesign som utvärderas i detta kandidatarbete ska kunna användas vid GSI.

En skiss över en del av experimentanläggningen vid GSI finns i figur 20. Joner produceras och skickas antingen till experiment i experimenthallen, eller vidare till synkrotronen SIS (SchwerIonen Synchrotron, tungjonssynkrotron), där de accelereras till relativistiska energier. Därefter skickas de direkt eller för exotisk sekundärjonproduktion och passage genom fragmentseparatorn (FRS) till en lagringsring (ESR, Experimental Storage Ring) eller en målhall. I figur 20 är målhall C utmarkerad [2, ss. 6-8]. Den detektor vi utreder är avsedd att placeras längst bak i målhallen för att inte blockera den normala experimentutrustningen.

### C.1.2 Existerande identifikationshjälpmedel

I nuläget finns det vid GSI en detektor, ITAG (Isomer TAGging detector), som är avsedd att detektera isomerer med en livslängd på mellan 100 ns och 1 ms [3]. De isomera tillstånden produceras främst för tyngre kärnor vid isotopproduktionen före FRS. De är en för själva experimenten oönskad komplikation eftersom de normalt inte kan urskiljas, och ankommer till experimentplatsen i okänt tillstånd. ITAG-detektorn fungerar i många avseenden på ett liknande sätt som den detektordesign som vi utreder. ITAG-detektorn

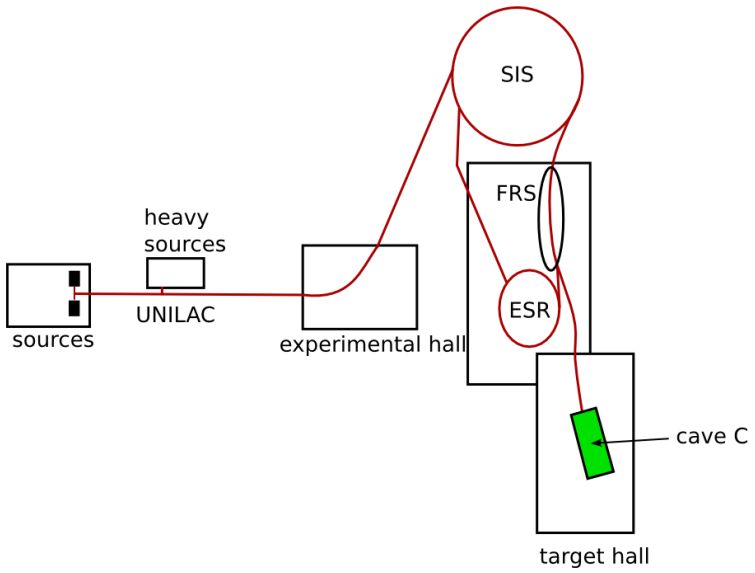


**Figur 20:** Skiss över en del av experiment- och acceleratoranläggningen vid GSI [2, p. 7]. Strållinjer är markerade i rött. FRS (svart ellips) och Cave C (grön rektangel) är markerade. Bilden är ej skalenlig.

bygger på att isomerer implanteras i ett därför avsett objekt. Därefter uppmäts energin hos $\gamma$-fotonerna som resulterar från isomerernas $\gamma$-sönderfall. Identifikationen görs genom att jämföra den uppmätta energin i gammafotonerna med en referenstabell [3]. En stor skillnad mellan ITAG-detektorn och den detektordesign som vi utreder i detta projekt är de partiklar som respektive detektor kan detektera. Medan ITAG-detektorn detekterar isomerer, kan detektordesignen som utreds i detta projekt detektera partiklar som har egenskapen att de betasönderfaller till exciterade tillstånd. Som figur 21 illusterarar så överlappar nukliderna som den föreslagna detektorn kan detektera endast i 22 av 107 fall med de som ITAG kan detektera.

En annan viktig skillnad är att den detektordesign som utreds här är avsedd att placeras bakom alla experimentuppställningar (och därför inte påverkar dessa), medan ITAG-detektorn placeras vid fragmentseparatorn på GSI. Således kan den i den här rapporten utredda designen även användas under själva experimentet för att säkerställa att man fortfarande har de partiklar man tror att man har, medan ITAG-detektorn inte kan användas samtidigt som det verkliga experimentet sker.

## C.2 Genomförande

Projektet genomfördes väsentligen med hjälp av datorbaserade beräkningar och simuleringar. Det dominerande språket som användes var C++, och för detektorsimuleringar användes ett verktyg benämnt `Geant4` [5].

Genomförandet kan indelas i flera steg. Det första är att identifiera och visualisera de

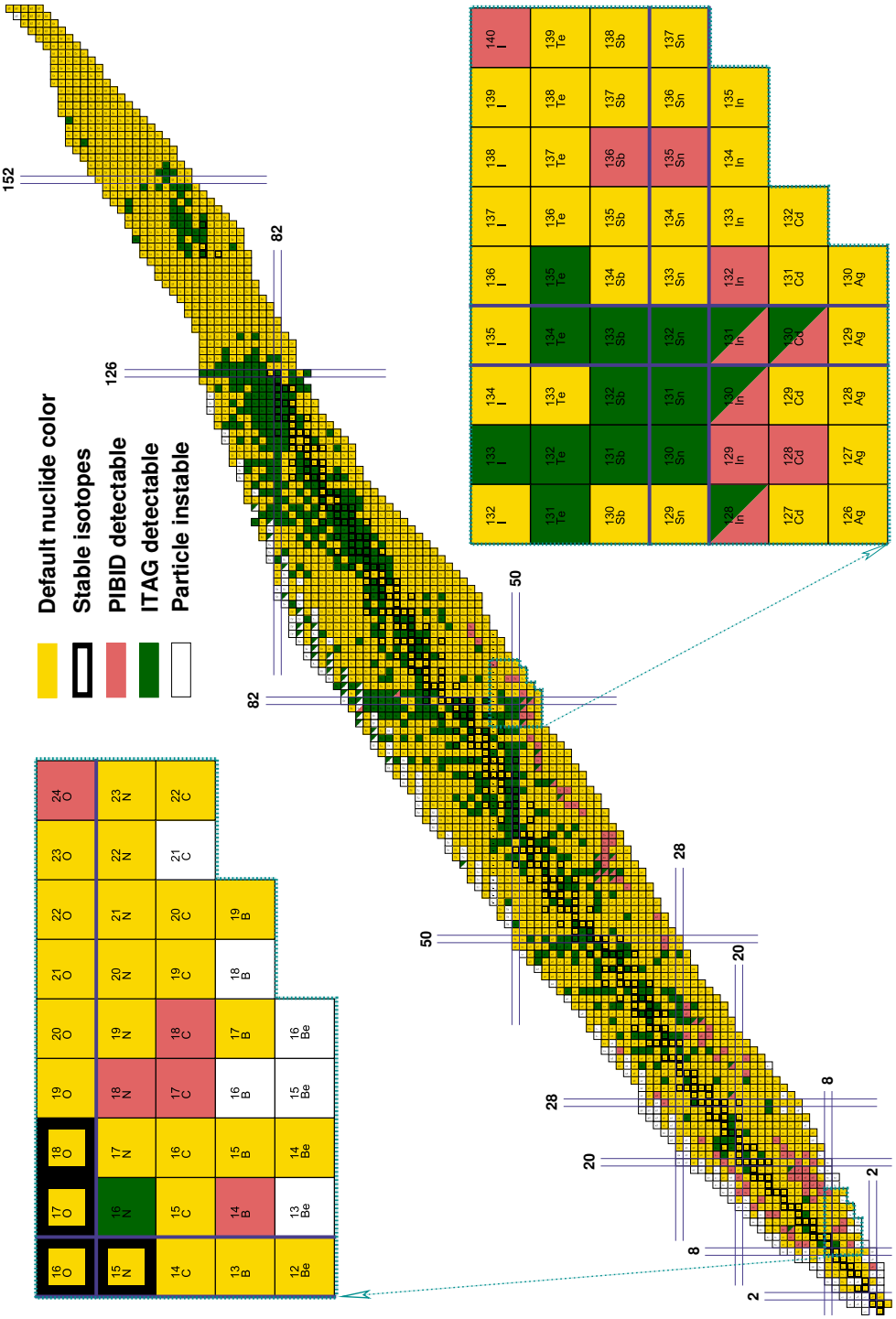


**Figur 21:** Nuklidkarta illustrerande isotoper detekterbara med den föreslagna detektorn (PIBID) och ITAG-detektorn. Färgkodningen är beskriven i figuren. Notera att nukliderna identifierbara med PIBID endast överlappar de nuklider som är identifierbara med ITAG i 22 av 107 fall.

nuklider som skulle kunna identifieras av den föreslagna detektorn i ENSDF-databasen. Med dessa var kända kan detektorn simuleras med `Geant4`, och resultaten analyseras.

### C.2.1 Identifikation av lämpliga nuklider

Ett program för att söka igenom ENSDF-databasen[12] utvecklades. Detta program skrevs i syfte att även kunna göra andra sökningar i ENSDF-databasen än de som krävdes för detta projekt. Detta program benämndes `ENSDF++`, och notervärt är att flera syntaxfel i ENSDF-databasen upptäcktes och korrigerades efter författarnas påpekande [23]. Programmet anpassades för att söka efter nuklider med beta-sönderfall följt av gammasönderfall, och halveringstider på mellan 1 ms och 1 s samt 10 % sannolikhet för utsändande av en gammafoton med en specifik våglängd användes som sökvillkor.

### C.2.2 Detektorsimulering och analys

Detektorn simulerades med hjälp av programbiblioteket `Geant4`. Simulerings-analysprocessen är illustrerad i figur 22. Simuleringsprogrammet kördes med en isotop åt gången, och utdata från körningar med olika isotoper blandades med ett program så att mer realistisk data erhölls för analys. Slutligen användes ett analysprogram för att analysera data på samma sätt som skulle skett med data från en verklig detektor.

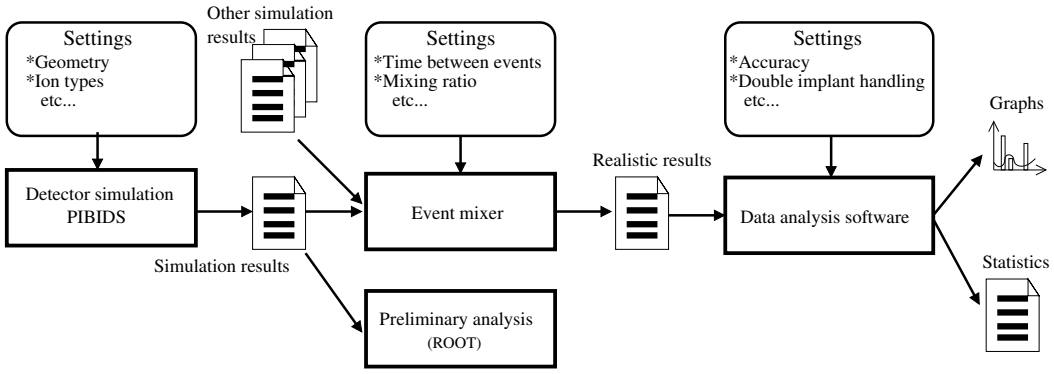


**Figur 22:** Skiss över simulerings-analys-processen.

## C.3 Den föreslagna detektorn

Syftet med detektordesignen är att tillhandahålla absolut information om jonsammansättningen hos partikelstrålar. Detektorn skall koppla samman de identifierade nuklidera med information om deras egenskaper i experimentuppställningen. Däremot förväntas den inte tillhandahålla information om alla nuklider som träffar — med den föreslagna designen kan den endast identifiera ett visst fåtal partiklar, men med hög noggrannhet.

[12] En hålkortsdatabas innehållande experimentellt uppmätta data om över 3000 olika nuklider.

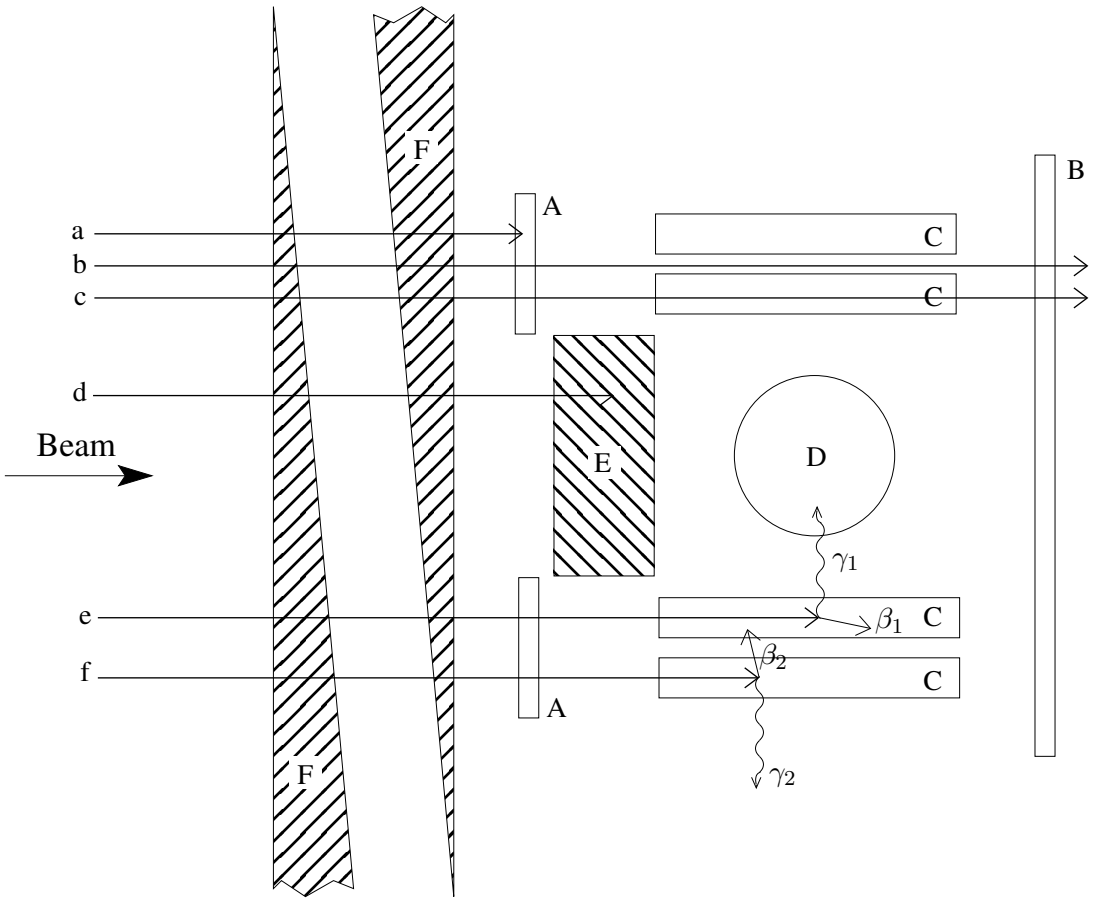


**Figur 23:** Skiss över detektorkonstruktionen. A och B är plattor av scintillatormaterial; C är en mängd cylindrar gjorda av scintillerande material placerade parallellt med strålriktningen, placerade sida vid sida i de fyra grupperingarna, C, i figuren; D är en germaniumkristall — en högupplösande gammadetektor; E är ett rektangulärt block av bly; F representerar kilar av aluminium. $a$ – $f$ är inkommande partiklar som interagerar med detektorn; $\beta_1$ och $\beta_2$ är elektroner resulterade från respektive $\beta$-sönderfall hos $e$ och $f$; $\gamma_1$ och $\gamma_2$ är $\gamma$-fotoner resulterande från de respektive $\gamma$-sönderfallen hos $e$ och $f$.

Då en partikelstråle riktas mot detektorn, så som illustreras i figur 23, så kan efter analys en lista av alla identifierade joner tillsammans med information som kopplar var och en av nukliderna till motsvarande händelser i experimentuppställningen genereras. På så sätt kan egenskaper uppmätta genom experimentet tilldelas varje identifierad jon.

I praktiken finns osäkerhet i jonidentifikationerna, och därför måste flera sådana sammankopplingar tillsammans med statistiska medel användas för att göra jon – experimentella egenskaper-associationen. Om detta lyckas så kan informationen användas för att göra absolutkalibreringar av huvudutrustningen i experimentuppställningen. Att kunna göra denna typ av kalibrering är syftet med detektorn i fråga.

Själva identifikationen av joner sker, i kronologisk ordning, genom följande process[13]:

1. ***Partikelegenskaper mäts upp i experimentuppställningen.***
2. ***Partiklarna implanteras i scintillatorrör*** i PIBID-detektorn. Genom att experiment – detektor-flygtiden är känd så är det möjligt att hålla reda på vilka partiklar som från experimentet som motsvarar vilka implantationer i scintillatorrören.
3. ***Partiklarna i scintillatorrören $\beta$-sönderfaller*** till kärnexciterade tillstånd, varefter de sänder ut varsin $\gamma$-fotoner i samband med sina respektive $\gamma$-sönderfall.
4. ***$\gamma$-fotonernas energier mäts upp*** av germaniumdetektorn, om de träffar den.
5. ***$\gamma$-energierna jämförs*** med kända värden listade i tabellverk — exempelvis tabellverket `ENSDF`.

## C.4 Resultat och analys

Ett flertal simuleringar genomfördes, och isotopen $^{17}$C användes i huvudsak. I ett fall användes även isotoper i dess omedelbara omgivning i nuklidkartan, och dessa blandades då ihop med $^{17}$C för att göra identifikationsprocessen mer realistisk. Det fanns flera anledningar till att $^{17}$C användes:

- Varken $^{17}$C eller dess omgivande nuklider är isomerer. Därför skulle ITAG-detektorn (se avsnitt C.1.2) inte kunna identifiera dessa.
- $^{17}$C är inte särskilt enkel att identifiera eftersom dess utsända gammafotoner har relativt låg sannolikhet, vilket bör ge mer realistiska resultat.
- $^{17}$C är en lätt kärna, vilket innebär att den torde vara av särskilt intresse för den forskning som utförs av Subatomär-gruppen på Chalmers Tekniska Högskola.

Kärnor som träffar detektorn har ett konstant $B\rho$-värde, vilket innebär att de alla har passerat ett konstant magnetfält med ungefär samma krökningsradie ($\rho$). Värdena på $B\rho$ beräknades för en infallande jon av en specifik jontyp som användes vid sammanblandningen, och därefter användes detta värde för att beräkna energierna hos övriga joner som träffade detektorn.

### C.4.1 Simuleringar i $^{17}$C-området

Simuleringar genomfördes med $2 \cdot 10^6$ joner vardera av isotoperna $^{16}$B, $^{16}$C, $^{16}$N, $^{17}$B, $^{17}$C, $^{17}$N, $^{18}$B, $^{18}$C och $^{18}$N med standardinställningar hos detektorn. Ett $B\rho$-värde på $B\rho \approx 12{,}08\,\mathrm{Tm}$ användes, vilket svarar mot en energi på $650\,\mathrm{MeV/u}$ för $^{17}$C [6]. Data från simuleringarna blandades med eventmixingsprogrammet med tider mellan jonerna som

[13] Givetvis har inte alla partiklar de egenskaper som krävs för att processen beskriven skall vara möjlig. Endast 107 sådana har identifierats och finns illustrerade i figur 21

sträckte sig över flera storleksordningar. Data analyserades därefter med dataanalysprogrammet, och olika inställningar (såsom hur dubbelimplantation hanterades) varierades. Det visade sig vara möjligt att identifiera $^{17}$C med god noggrannhet om de träffande jonerna spreds ut över ungefär 13 timmar, men om intensiteten ökades för mycket så minskade noggrannheten. Av de övriga nukliderna var även $^{18}$C och $^{18}$N identifierbara med den förkalibrerade jonstrålidentifikationsdetektorn. Identifikation av dessa var dock svår, då färre events erhölls, troligtvis på grund av att dessa inte stannade på samma ställe i detektorn som $^{17}$C-atomerna innan de sönderföll då de hade en annan energi. Identifikationsspektra kan betraktas i figur 24.

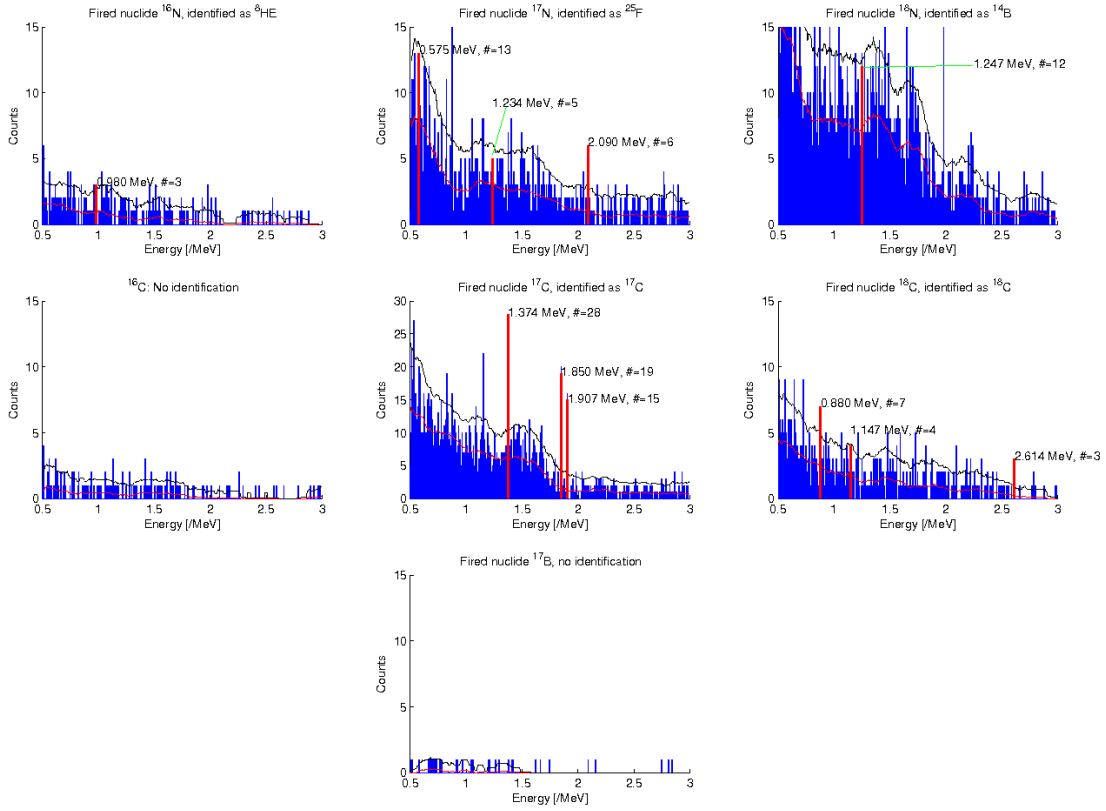


**Figur 24:** Identifikationsplot för $^{17}$C, med en intensitet på 140 events per sekund i 13 timmar och 27 minuter, vilket svarar mot $1{,}8 \cdot 10^6$ joner. Den röda linjen är ett glidande medelvärde och den svarta linjen är medelvärde plus två standardavvikelser.

### C.4.2 Variation av detektorparametrar

Simuleringar genomfördes med $^{17}$C under vilka en av detektorns parametrar varierades, detta i syfte att studera hur detektorns prestation berodde av dess geometri.

**Scintillatorrörens diameter** Diametern hos scintillatorrören minskades i förhoppning om att kunna öka partikelstrålens intensitet och öka antalet rör på samma yta, så att identifikationen skulle kunna gå snabbare. En minskad diameter ledde dock till ökat antal felidentifikationer, vilket tros bero på ökat antal implantationer i skyddet mellan scintillatorerna.

**Tjocklek på skyddet mellan scintillatorrören** Tjockleken på skyddet mellan scintillatorerna ändrades med samma avsikt som ovan. Denna ändring ledde dock till att spektra blev sämre för de högre intensiteterna.

**Materialet hos skyddet mellan scintillatorrören** Materialet hos skyddet mellan scintillatorrören (som fanns där för att förhindra att elektronerna från $\beta$-sönderfallen åkte mellan dessa) ändrades för att utvärdera huruvida järn, kvarts eller aluminium var mest lämpligt i detta syfte. Det visade sig att kvarts skyddade sämst och järn bäst, men samtidigt så minskade antalet gammafotoner som detekterades av germaniumdetektorn, vilket givetvis inte är bra.

**Skydd framför skyddet mellan scintillatorerna** Ett skydd av bly placerades framför skyddet mellan scintillatorerna i syfte att förhindra implantation i detta. Ett tunt sådant skydd verkar öka antalet korrekt identifierade och sammankopplade gammafotoner, ett tjockt minskar dock antalet. Det sistnämnda beror troligtvis på att den tillåtna vinkelspridningen hos joner i partikelstrålen minskar då tjockleken ökar.

**Radie hos germaniumdetektorn** I syfte att minska Comptonspridningen testades större radier på germaniumdetektorn. Detta ledde dock snarare till ett sämre än ett bättre gammaspektrum, vilket skulle kunna bero på att fler elektroner och andra partiklar än gammafotoner träffar detektorn. Denna idé torde därför inte vara att rekommendera.

## C.5 Framtiden

Utvärderingen av detektordesignen har visat lovande resultat, men den matchar ännu inte tidskraven för ett verkligt experiment. För att det skulle utgöra en praktisk fördel framför existerande metoder, så skulle detektorn behöva göra identifieringen på runt en timma. I nuläget verkar identifikationen av $^{17}$C ta ungefär 10 gånger så lång tid. Framtida studier kommer att få avgöra huruvida det går att förbättra detektordesignen så att detta mål kan uppnås. Dessa studier skulle kunna undersöka om det går att förändra detektordesignen för att öka dess effektivitet, eller att förbättra de algoritmer som används för analys av data från detektorn. Det förstnämnda skulle exempelvis kunna göras genom att ändra olika detektorparametrar såsom scintillatorrörens längd eller skyddet runt germaniumdetektorn, det sistnämnda skulle exempelvis kunna ske genom att skatta halveringstiden för implanterade nuklider och jämföra med kända värden.

## C.6 Slutsats

En detektor avsedd att identifiera joner i en partikelstråle har undersökts. Undersökningen var en flerstegsprocess som inkluderade skapandet av ett sökprogram för en nuklid-databas, identifikation av nuklider lämpliga för att identifieras i detektorn, simuleringar av detektorn samt analys av simulerad data.

Det visade sig att det med en tillräckligt låg intensitet på partikelstrålen (140 events/s) är möjligt att identifiera merparten av $^{17}$C-jonerna i en stråle sammansatt av flera olika nuklider under en total tid på ungefär 13 timmar. Detta är ungefär en storleksordning för mycket jämfört med projektets målsättning. Huruvida det är möjligt att vidareutveckla designen och därigenom öka effektiviteten kommer att behöva avgöras av framtida studier.